NASA TN D-1933

49p.

TECHNICAL NOTE

D-1933

EFFECT OF FABRICATION-TYPE SURFACE ROUGHNESS ON TRANSITION ON OGIVE-CYLINDER MODELS AT MACH NUMBERS OF 1.61 AND 2.01

By Paul W. Howard and K. R. Czarnecki

Langley Research Center
Langley Station, Hampton, Va.

NATIONAL AERONAUTICS AND SPACE ADMINISTRATION
WASHINGTON July 1963

NATIONAL AERONAUTICS AND SPACE ADMINISTRATION

TECHNICAL NOTE D-1933

EFFECT OF FABRICATION-TYPE SURFACE ROUGHNESS ON TRANSITION ON OGIVE-CYLINDER MODELS AT MACH NUMBERS OF 1.61 AND 2.01

By Paul W. Howard and K. R. Czarnecki

SUMMARY

An investigation has been made at Mach numbers of 1.61 and 2.01 over a range of free-stream Reynolds number per foot from about 0.5×10^6 to 4.5×10^6 to determine the effects of fabrication-type surface roughness on boundary-layer transition. Twelve types of surface roughness, including step, wave, crease, waffle, hemstitching, and swept configurations, were investigated. The tests were made on an ogive-cylinder body of fineness ratio 12.2, the roughness elements covering the cylindrical portion of the model.

The results indicate that there was little or no difference in transition characteristics for the hemstitching and smooth-waffle type of surface roughness. For most of the other types of roughness configurations, surface roughness decreases the transition distance by approximately a constant percentage over the test Reynolds number per foot range. Transition distance decreases nearly linearly with roughness height for two-dimensional, protruding, unswept type of surface roughness. Generally, roughness shape has relatively small effects on transition and Mach number has a small favorable effect. Sweptback type of surface roughness appears to have a larger detrimental effect on transition than the transverse or unswept type.

INTRODUCTION

Knowledge of boundary-layer transition has always been of importance to the designer of supersonic aircraft. Recently, however, there has been a strong tendency to downgrade the significance of laminar flow. The trend toward the development of supersonic aircraft flying at very high altitudes at low free-stream Reynolds numbers per foot, however, can lead to significant runs of laminar boundary-layer flow near wing leading edges and fuselage noses if the surfaces are smooth. Unfortunately, at these supersonic flight conditions, frictional heating will tend to distort the surfaces, and the resulting surface roughness will tend to precipitate transition to turbulent flow. It appears desirable, therefore, to explore the possible magnitude of the effects of fabrication-type

surface roughness on transition at supersonic speeds and to establish limits wherein the effects may be reasonably small.

The transition tests were made on 12 types of fabrication roughness built into the cylindrical portion of an ogive-cylinder model having a fineness ratio of 12.2. Both two- and three-dimensional-shaped roughnesses were investigated. The tests were made at nominal Mach numbers of 1.61 and 2.01 over a range of free-stream Reynolds number per foot from about 0.5×10^6 to 4.5×10^6. The model longitudinal axis was always alined with the free stream. Transition location was determined by schlieren photography and typical schlieren photographs of the flow over the roughness elements in the transitional phase are included.

SYMBOLS

C_p pressure coefficient, $\frac{p_l - p_\infty}{q_\infty}$

h height of surface roughness

M free-stream Mach numbers

p_l local static pressure

p_∞ free-stream static pressure

q_∞ free-stream dynamic pressure, $0.7p_\infty M^2$

r radius of ogive

R_{FT} free-stream Reynolds number per foot

R_{x_t} transition Reynolds number based on free-stream conditions and axial distance to transition

x axial distance measured from tip of model nose

x_t axial distance to transition

$x_{t,s}$ axial distance to transition on average "smooth" body

APPARATUS AND TESTS

Wind Tunnel

This investigation was conducted in the Langley 4- by 4-foot supersonic pressure tunnel at Mach numbers of 1.61 and 2.01. Calibrations of flow in the test

section indicate that the Mach number variations about the mean value of free-stream Mach numbers are about ±0.01 in the region occupied by the model and that there are no significant pressure gradients or flow irregularities in stream flow direction.

Models

A 50.0-inch-long 4.096-inch-diameter 3-caliber-nose ogive-cylinder model was the basic configuration of the 14 sting-mounted models tested. All models were smooth in the ogival nose sections. Two of the models, used only to establish the basic pressure gradients on the test models, had no roughness elements. (See fig. 1.) One of these models had a plain ogival nose; the other had a 6.5-inch-long pitot-static probe extending from its ogival nose. Both models were instrumented with approximately three-dozen static-pressure orifices (see table I) in a single row parallel to the model center line. The remaining 12 configurations had a number of cycles of a particular type of fabrication roughness constructed into the cylindrical portion of each body. (See figs. 2 and 3 for photographs and detail sketches for most of the configurations investigated.) These roughness types included longitudinal and circumferential rows of roughness resembling hemstitching (usually the product of welding a thin skin to stringers or ribs), a waffle-like surface (resulting from heating a thin skin mounted on a honeycomb core), grooves, forward-facing steps, steps with grooves, creases, and protruding waves. Each roughness had a nearly constant cycle length, varying from about 0.4 inch for waffle-like roughness to a range of 1.5 to 2.0 inches for the step- and wave-type configurations, and an approximately constant height ranging from indentations of about 0.0015 inch for the hemstitching models to ridges of 0.053 inch for some of the wave configurations. The heights of the various roughness elements were selected to be representative of fabrication imperfections found on recent production transonic aircraft of aluminum construction, and the cycle lengths were chosen, in the case of the step, wave, and groove models, to provide enough cycles on the models (table II) to obtain a measurable difference in drag in balance tests (the results of which were previously reported in ref. 1). On eight of these models the roughness cycles were wrapped around the model unswept, on one model the roughness was swept 45°, and on two models the surface roughness was installed parallel to the model longitudinal axis. In the case of the three-dimensional waffle-like roughness, orientation angle has little meaning. Since it is difficult to illustrate the waffle or hemstitching type of roughness, no sketches are shown for these configurations. It should be mentioned, however, that both waffle models had irregular hexagonal lattices of ridges with spacings of about 0.25 and 0.30 inch between parallel ridges. The smooth-waffle model had a rather gently wavy surface with waves approximately 0.002 inch in height; whereas, the coarse-irregular-waffle model had rather sharp ridges which varied in height from as little as 0.001 inch to a maximum of about 0.006 inch, with an average value of more than 0.004 inch. The hemstitching models consisted of rows of dimples or indentations varying from a few ten-thousandths of an inch to a maximum of 0.0015 inch in depth, with the rows spaced about 0.4 inch apart.

The plain pressure-distribution ogive-cylinder model was constructed of aluminum. The remaining models were made of wood covered with plastic and fiber glass; however, the probe, as well as the first 2 inches of the nose, of each of

the fabrication-roughness ogive-cylinder models was aluminum in order to minimize tip damage. The surface finish of all models except that of the plain ogive-cylinder model was very smooth, usually less than 10 microinches. The plain ogive-cylinder model had a root-mean-square surface roughness of 85 microinches, but this roughness had no effect on surface pressure.

Tests and Techniques

All models were sting supported from the rear and all tests were conducted at zero angle of attack with zero heat transfer. The tests were conducted at Mach numbers of 1.61 and 2.01 over a range of Reynolds number per foot from 0.5×10^6 to 4.5×10^6 with the exception of the pressure models which were tested to a higher Reynolds number per foot of 8.24×10^6. During the tests, the dewpoint was kept below -20° F so that the effects of water condensation in the supersonic nozzle would be negligible.

The test procedure generally consisted of starting the tunnel at low stagnation pressures and advancing to the higher pressures. At intervals in tunnel pressure dictated by the movement of the transition front on the model, the tunnel pressure and temperature were stabilized and a group of about six to eight schlieren photographs were taken with the knife edge parallel to the tunnel axis. Transition distances were measured from the negatives, and an average value was computed for both the upper and lower surfaces of the model at each tunnel pressure and treated as a single point.

RESULTS AND DISCUSSION

Pressure Distributions

The type of pressure gradients existing on the basic smooth test model will, of course, have a strong influence on the transition characteristics. The nature of these gradients can be seen from the pressure distributions presented in figures 4 and 5 for the two test Mach numbers. At both Mach numbers there is an adverse pressure gradient beginning at the shoulder of the model where the ogive fairs into the cylindrical afterbody and continuing to about the 40-inch station. This adverse pressure gradient tends to become weaker as the distance from the model shoulder increases. Beyond about the 40-inch station, the pressure gradien appears to become approximately neutral at $M = 1.61$ and slightly favorable at $M = 2.01$.

The changes in local pressure gradients generated by the inclusion of the various roughness elements on the cylindrical portion of the model were not determined for these tests. For the two-dimensional-shaped roughness, these changes in pressure distribution can be found in reference 2 for the case of the turbulent boundary layer. It may be expected that for the case of laminar flow, these local pressure distributions will be considerably modified.

Schlieren Photographs of Flows

Some typical schlieren photographs of the boundary-layer flow over the roughness are presented in figures 6 and 7. One of the primary features of this group of photographs is that when the boundary layer is laminar the flow disturbances generated by surface roughness either cannot be discerned or are weak and diffuse. For the models with the wave types of roughness, the laminar boundary apparently separates and does not flow into the valleys or troughs but effectively smooths out the surface contours (figs. 7(h) and 7(i)). Where the boundary layer becomes turbulent, the flow follows the surface contours more closely and the resulting flow disturbances become stronger and more concentrated. For the step models (figs. 6(d), 7(f), and 7(g)), the flow separations are difficult to see, but it is well known that the separation and reattachment angles (for example, see ref. 3) are considerably smaller than those for the turbulent boundary layer. Thus, the laminar boundary layer again effectively smooths out the surface contours. In the case of three-dimensional-shaped roughness (figs. 6(b) and 7(c)), the stronger flow disturbances outside the boundary layer in the turbulent-flow case can be ascribed to the higher boundary-layer velocities close to the surface compared with those for the laminar-flow case.

Transition Distance

The effects of fabrication-type surface roughness on transition distance are shown in figures 8, 9, and 10. In these figures the transition distance x_t is plotted against free-stream Reynolds number per foot R_{FT} for each roughness configuration.

The data for the models with smooth-waffle, coarse-longitudinal-hemstitching, and coarse-circumferential-hemstitching types of surface roughness have been plotted in figure 8 at $M = 2.01$. At $M = 1.61$, data were available for only one model in this group (fig. 9(a)). These data (figs. 8 and 9(a)) indicate that there was little or no difference in the transition-distance characteristics. They also indicate the longest transition distance characteristics with increase in free-stream Reynolds number per foot and were used to establish the reference curve presented in figures 9 and 10. It is believed that these data represent transition on an essentially smooth surface inasmuch as, for maximum surface-roughness variation from 0.0015-inch indentations for the hemstitching models to about 0.006-inch projections for the waffle-surface models, there is no change in transition characteristics over the range of Reynolds numbers per foot investigated. There was apparently no measurable effect of Mach number on these so-called "smooth" bodies. (Compare fig. 8 with fig. 9(a).)

Included in figure 8 is a line for transition distance at constant transition Reynolds number. Comparison of the experimental results with this line indicates that R_{x_t} increases as R_{FT} increases. For transition located at the model base (low R_{FT}), the value of R_{x_t} is about 3×10^6; at the maximum test Reynolds number per foot, the transition Reynolds number R_{x_t} had increased to nearly 8×10^6. This increase in R_{x_t} occurs as the transition location moves

into a region of stronger adverse pressure gradient but a shorter run of this gradient. (See fig. 4.) On the smooth-waffle model at $M = 1.61$ (fig. 9(a)), transition moved abruptly forward to the model shoulder at an R_{FT} of about 4×10^6. This abrupt forward movement is ascribed to surface-roughness effects resulting from sandblasting of the soft ogival portion of the model with particles of grit. The sandblasting problem grows more acute with increase in tunnel pressure.

In these "smooth" model tests (figs. 8 and 9(a)), transition at the model base occurs at somewhat lower values of R_{FT} than indicated for the smooth model in reference 4. This discrepancy can be explained, at least partly, by the differences in methods of determining transition. Schlieren photographs tend to indicate earlier appearance of transition; whereas the force tests and base pressures, as interpreted in reference 4, tend to indicate transition only after it has progressed sufficiently to have a discernible effect on the skin friction or base pressure.

For models other than the ones with smooth waffle, coarse longitudinal hemstitching, or coarse circumferential hemstitching (the so-called "smooth" models), the usual effect of fabrication-type surface roughness was to decrease the transition distance by approximately a constant percentage over the test R_{FT} range. (See figs. 9 and 10.) The effects were slightly smaller at Mach number 2.01. The approximately constant percentage decrease in transition distance appears to hold despite the fact that at higher values of R_{FT} the boundary layer has negotiated a much smaller number of roughness cycles. Apparently, the increase in the ratio of roughness height to boundary-layer thickness at the higher test R_{FT} conditions tends to compensate for the smaller number of roughness cycles involved. Also, the movement of transition to a region of stronger adverse pressure may have an influence.

For the case of the model with the 0.059-inch longitudinal grooves (fig. 9(c)), there was a change from the usual transition pattern. There was apparently little effect of the longitudinal grooves on transition at low values of R_{FT} but, at high values of R_{FT}, transition distance decreased markedly. Also, for some of the roughness configurations, there was a tendency for transition to move abruptly forward to the neighborhood of the foremost roughness element and even ahead of it at the high values of R_{FT}. (For example, see figs. 9(e), 9(f), 10(e), and 10(f).) For several of the configurations, at least, this effect is ascribed to sandblasting effects on the ogival nose of the model.

The ratio of transition distance for the model with protruding waves, creases, or step type of roughness to that for the average "smooth" body is plotted in figure 11 as a function of roughness height. Data for the models with coarse irregular waffle and longitudinal grooves have been omitted inasmuch as for the first type the roughness is three-dimensional and for the second type the ratio is dependent upon R_{FT}. Data for the model with transverse grooves have also been omitted because the effects of indentations on transition

are different from the effects of protuberances. Figure 11 indicates that for the two-dimensional, protruding, unswept type of surface roughness, the transition-distance ratio decreases nearly linearly with increase in roughness height. Roughness shape generally has relatively small effects on transition. The data generally indicate a small favorable effect of Mach number on transition distance for the same model. For the model with the swept type of roughness (0.020-inch 45° rearward steps), the decrease in $x_t/x_{t,s}$ is much larger than for the models with the unswept type roughness and with approximately the same roughness height. This indicates the probability that the swept type of two-dimensional surface roughness will have a larger detrimental effect on transition than the unswept type.

SUMMARY OF RESULTS

An investigation has been made at Mach numbers of 1.61 and 2.01 over a Reynolds number per foot range from 0.5×10^6 to 4.5×10^6 of the effects of fabrication-type surface roughness on boundary-layer transition on a 50-inch ogive-cylinder model of fineness ratio 12.2. The following results were indicated for the types of roughness configurations tested:

1. There was little or no difference in transition-distance characteristics for the hemstitching and smooth-waffle types of surface roughness.

2. For most of the other types of roughness configurations, surface roughness decreases the transition distance by approximately a constant percentage over the test Reynolds number per foot range.

3. Transition distance decreases nearly linearly with roughness height for two-dimensional, protruding, unswept type of surface roughness.

4. Roughness shape generally has relatively small effects on transition.

5. Generally, there is a small favorable effect of Mach number on transition.

6. Sweptback type of surface roughness appears to have a larger detrimental effect on transition than the transverse or unswept type.

Langley Research Center,
National Aeronautics and Space Administration,
Langley Station, Hampton, Va., May 1, 1963.

REFERENCES

1. Czarnecki, K. R., Sevier, John R., Jr., and Carmel, Melvin M.: Effects of Fabrication-Type Roughness on Turbulent Skin Friction at Supersonic Speeds. NACA TN 4299, 1958.

2. Czarnecki, K. R., and Monta, William J.: Pressure Distributions and Wave Drag Due to Two-Dimensional Fabrication-Type Surface Roughness on an Ogive Cylinder at Mach Numbers of 1.61 and 2.01. NASA TN D-835, 1961.

3. Chapman, Dean R., Kuehn, Donald M., and Larson, Howard K.: Investigation of Separated Flows in Supersonic and Subsonic Streams With Emphasis on the Effect of Transition. NACA Rep. 1356, 1958. (Supersedes NACA TN 3869.)

4. Czarnecki, K. R., Robinson, Ross B., and Hilton, John H., Jr.: Investigation of Distributed Surface Roughness on a Body of Revolution at a Mach Number of 1.61. NACA TN 3230, 1954.

TABLE I.- BASIC-MODEL ORIFICE LOCATIONS

Orifice	x, in.	
	Plain model	Probe-nose model
1	1.01	1.01
2	1.95	1.93
3	2.82	2.84
4	3.81	3.83
5	4.78	4.84
6	5.78	5.85
7	6.76	6.84
8	7.76	7.83
9	8.77	8.82
10	9.79	9.81
11	10.78	10.83
12	11.80	11.82
13	12.78	12.83
14	13.77	13.83
15	14.78	14.82
16	15.78	15.81
17	16.78	16.82
18	17.75	17.81
19	18.79	18.81
20	19.78	19.82
21	20.78	20.82
22	22.75	22.83
23	24.74	24.82
24	26.77	26.82
25	28.76	28.62
26	30.77	30.83
27	32.76	32.82
28	34.78	34.80
29	36.79	36.81
30	42.14	38.82
31	44.10	40.80
32	46.08	42.82
33	48.08	44.79
34	49.62	46.81
35		48.82

TABLE II.- MODEL DESCRIPTIONS

Description of ogive-cylinder models	Number of cycles of roughness
Plain (85 microinches, smooth)	---------
Probe nose (smooth)	---------
Coarse circumferential hemstitching	---------
Coarse longitudinal hemstitching	---------
Smooth waffle	---------
Coarse irregular waffle	---------
0.056-inch transverse grooves	37
0.059-inch longitudinal grooves	12
0.010-inch steps with grooves	9
0.020-inch forward steps	18
0.021-inch rearward steps	18
0.020-inch 45° rearward steps	5 stripes
0.053-inch protruding waves	24
0.053-inch transverse creases	24

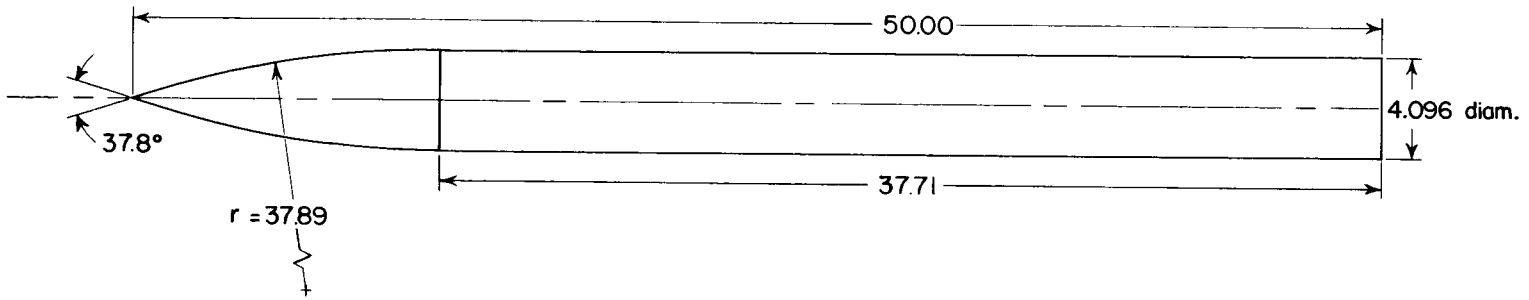

(a) Plain ogive-cylinder model.

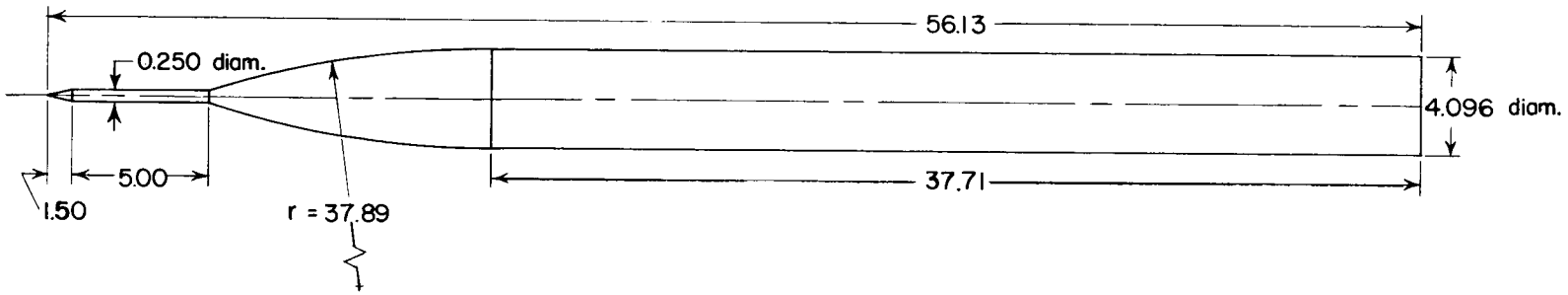

(b) Ogive-cylinder model with pitot-static probe.

Figure 1.- Sketch of basic models. All dimensions are in inches unless otherwise stated.

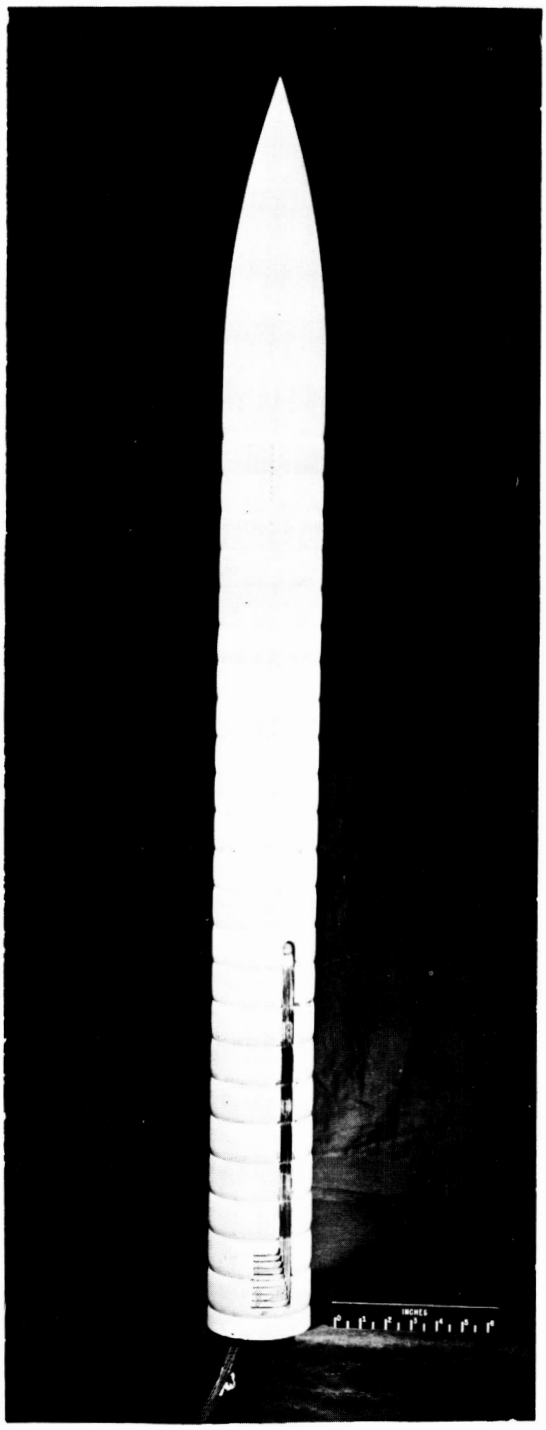

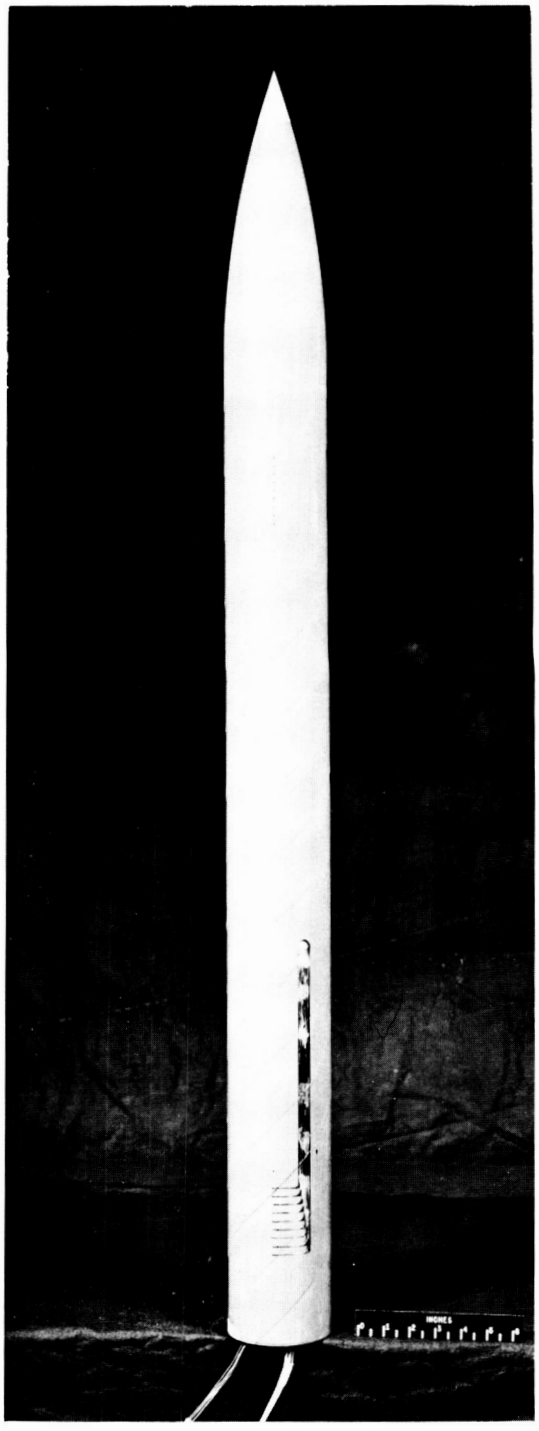

L-61-1039

(a) 0.053-inch transverse creases.

(b) 0.020-inch 45° rearward steps.

Figure 2.- Photographs of typical roughness models.

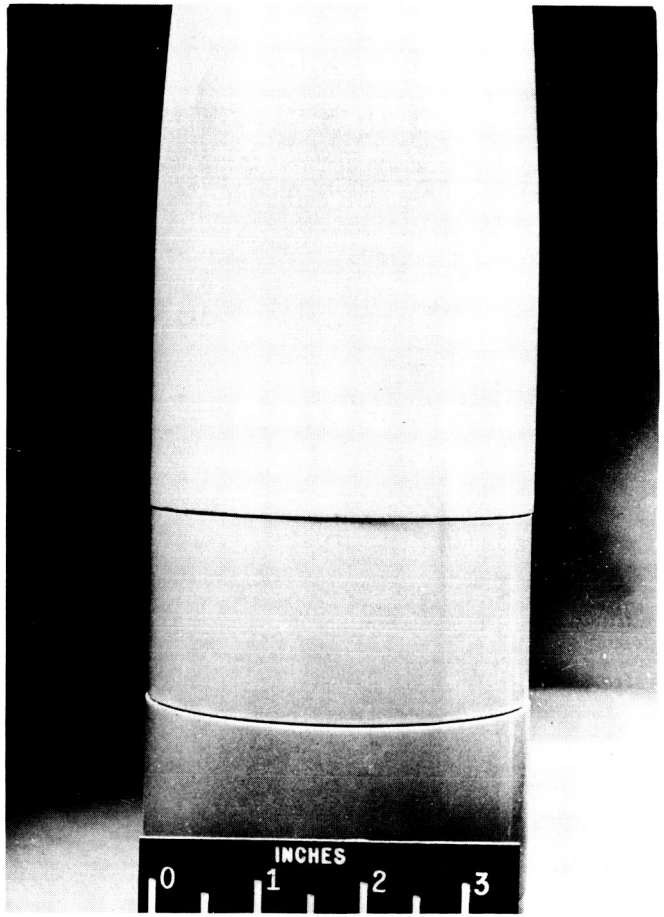

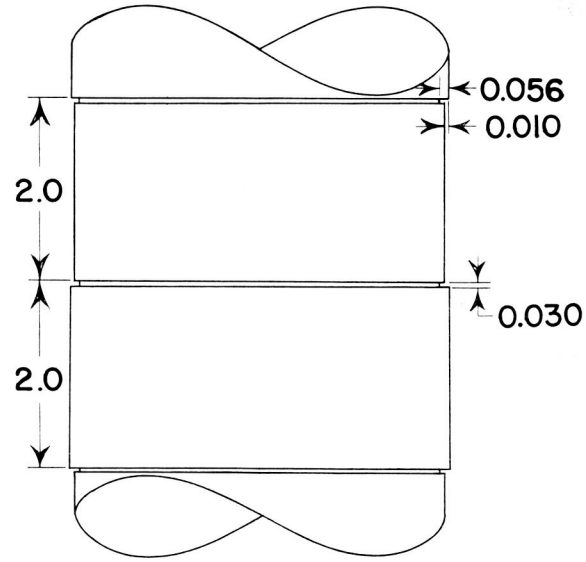

(a) 0.010-inch steps with grooves. L-61-1040

Figure 3.- Details of fabrication-type roughnesses. All dimensions are in inches unless otherwise stated.

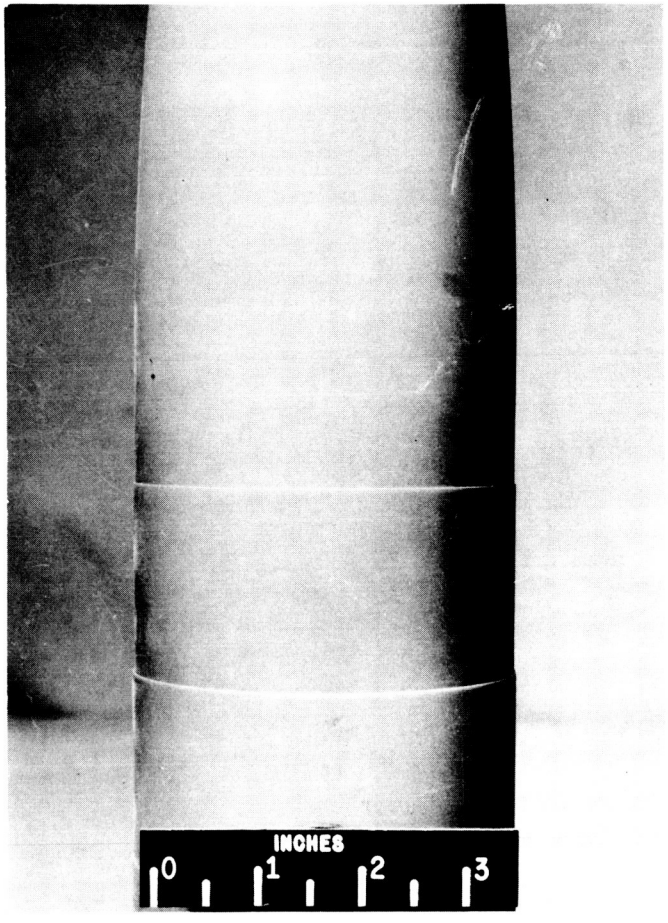

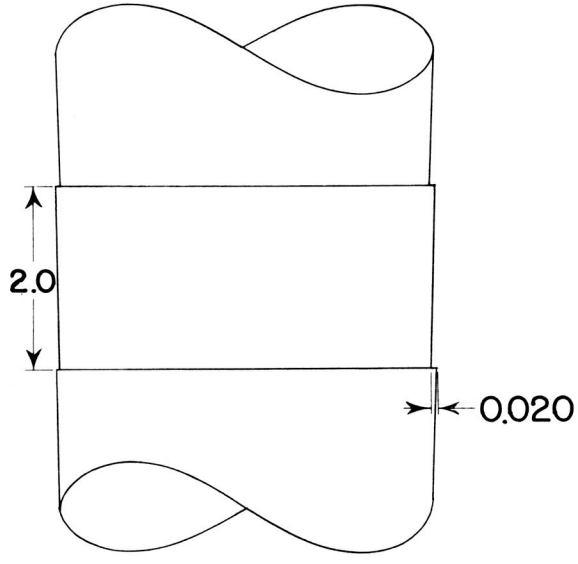

(b) 0.020-inch forward steps. L-61-1041

Figure 3.- Continued.

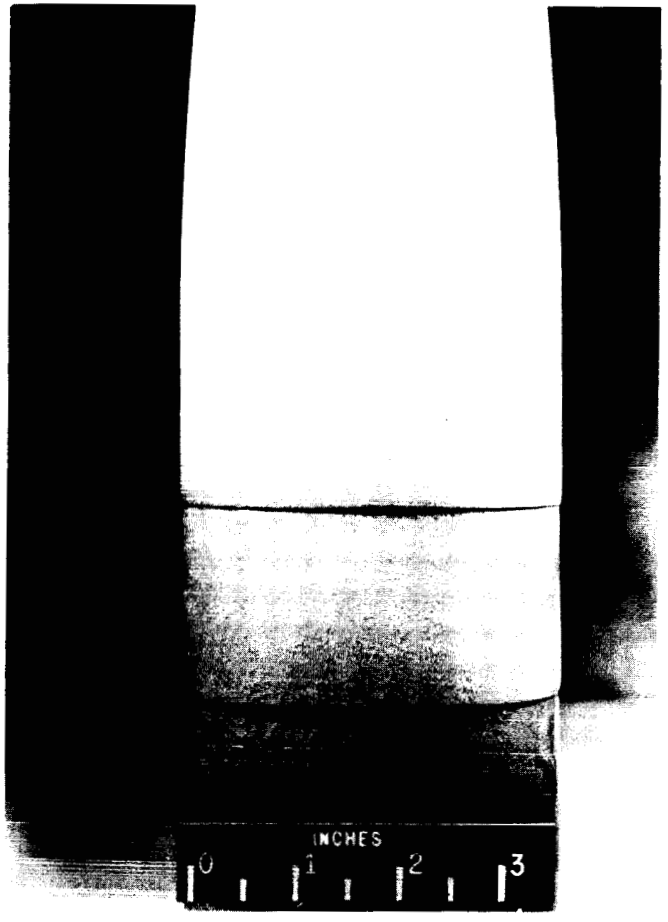

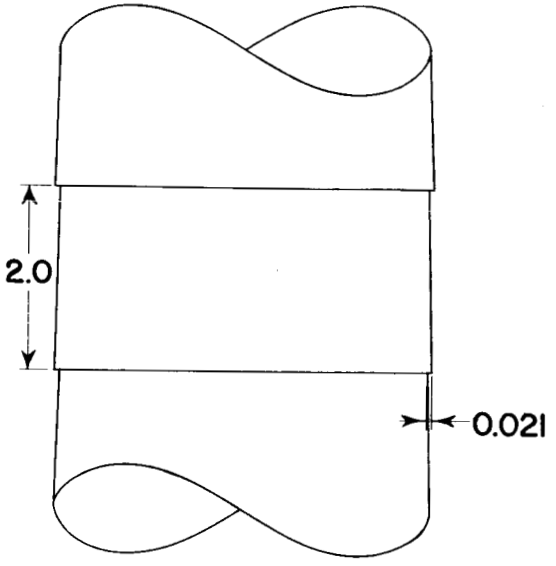

(c) 0.021-inch rearward steps.

L-61-1042

Figure 3.- Continued.

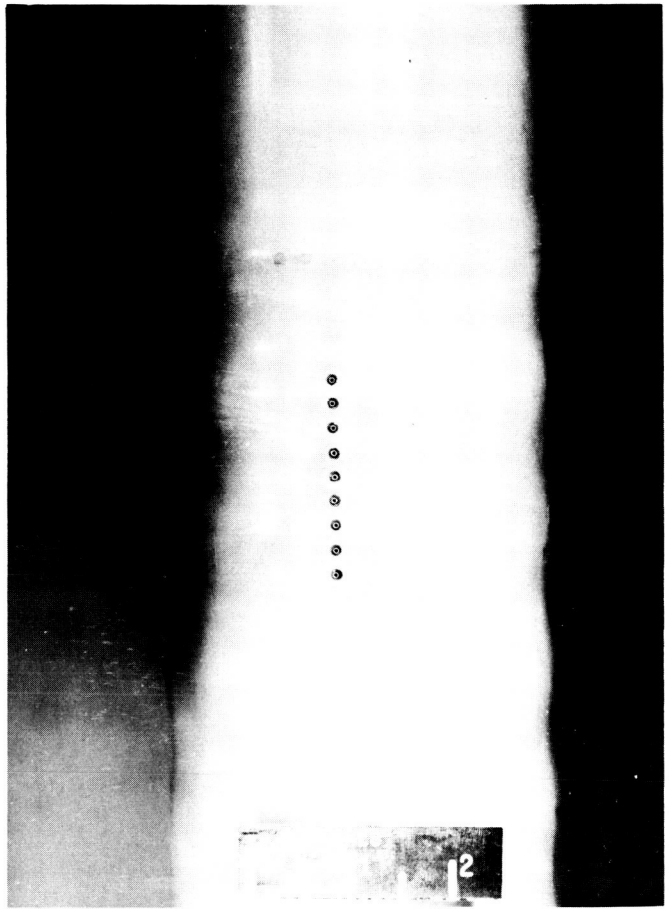

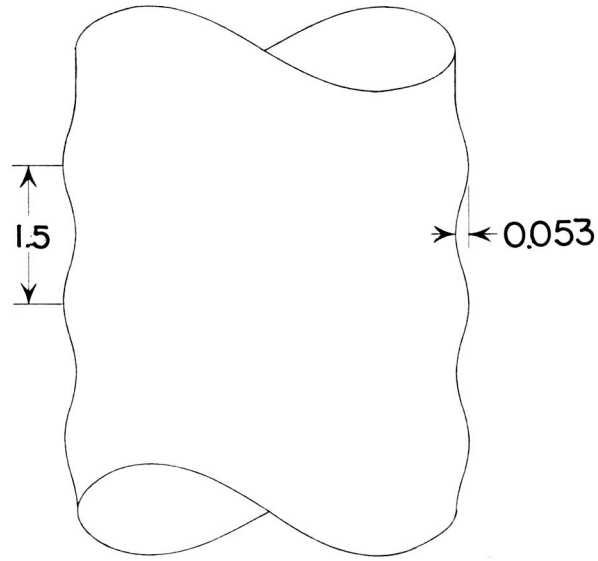

(d) 0.053-inch protruding waves.

L-61-1043

Figure 3.- Continued.

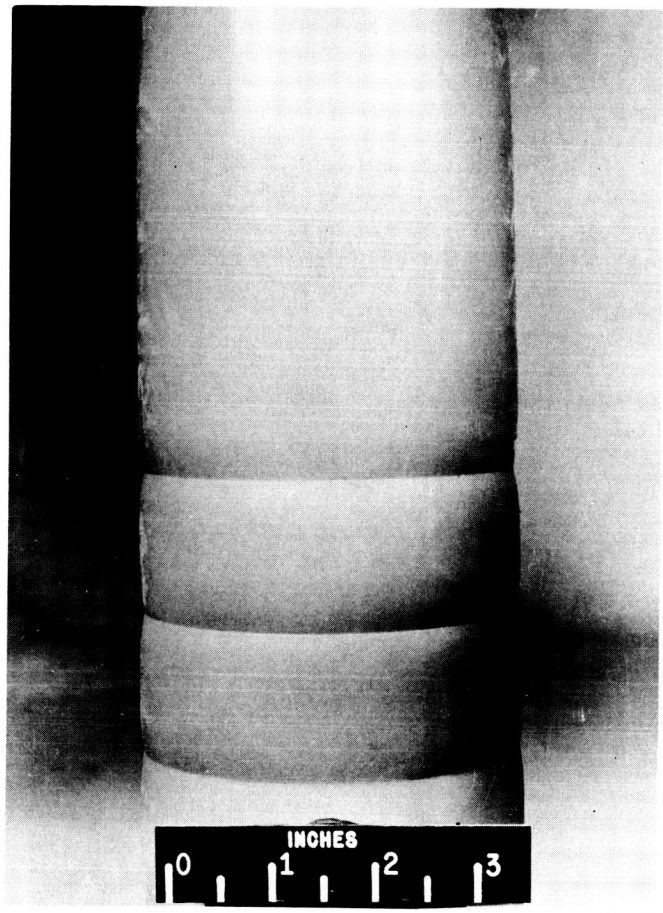

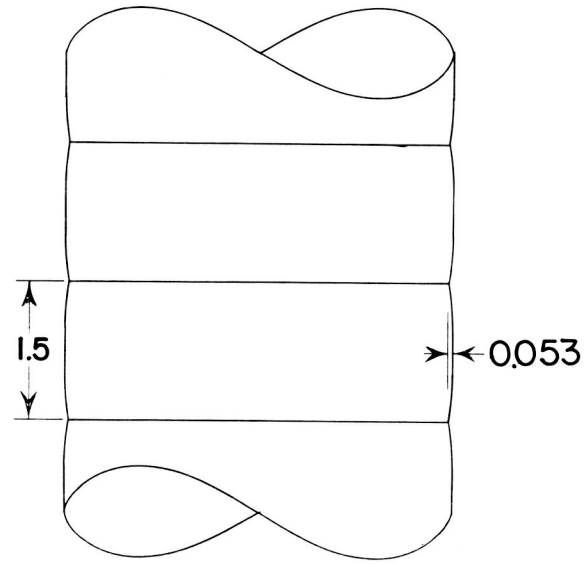

(e) 0.053-inch transverse creases. L-61-1044

Figure 3.- Continued.

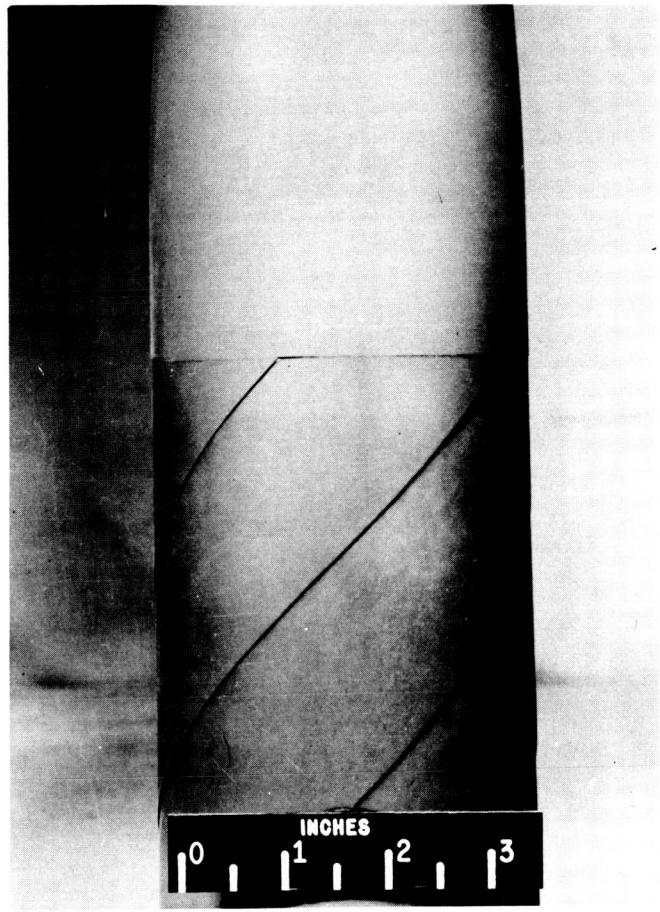

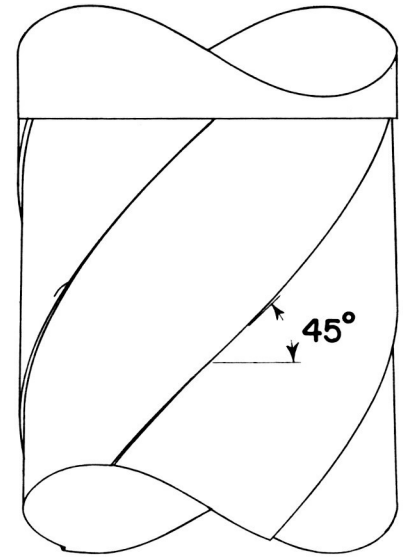

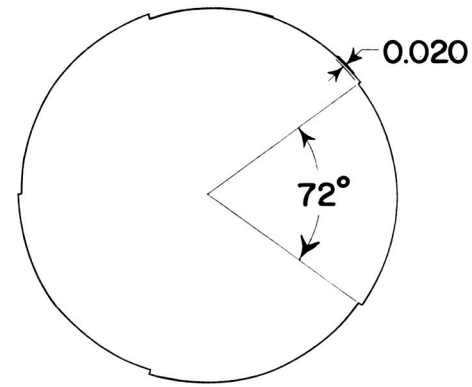

(f) 0.020-inch 45° rearward steps. L-61-1045

Figure 3.- Continued.

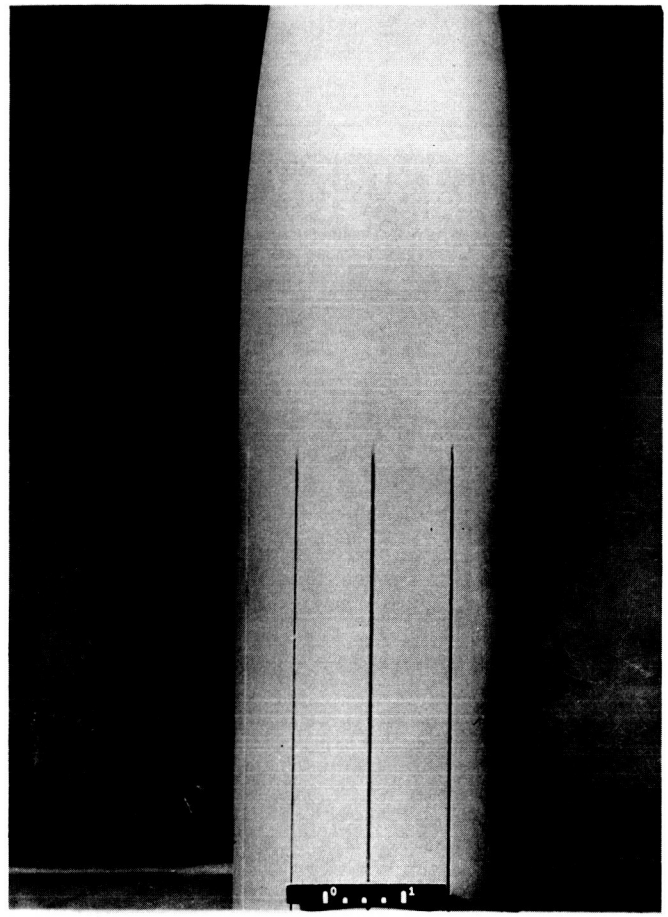

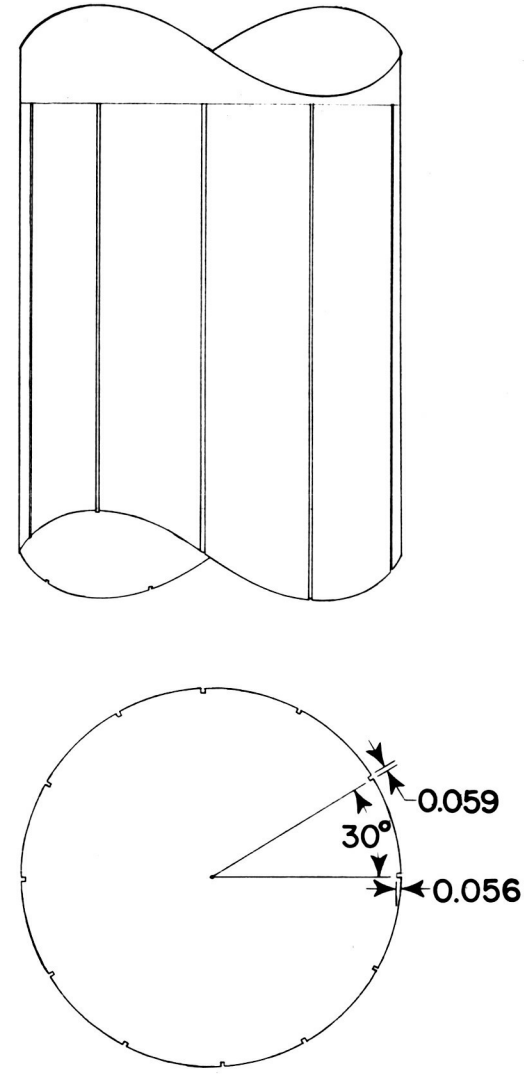

(g) 0.059-inch longitudinal grooves. L-63-3119

Figure 3.- Continued.

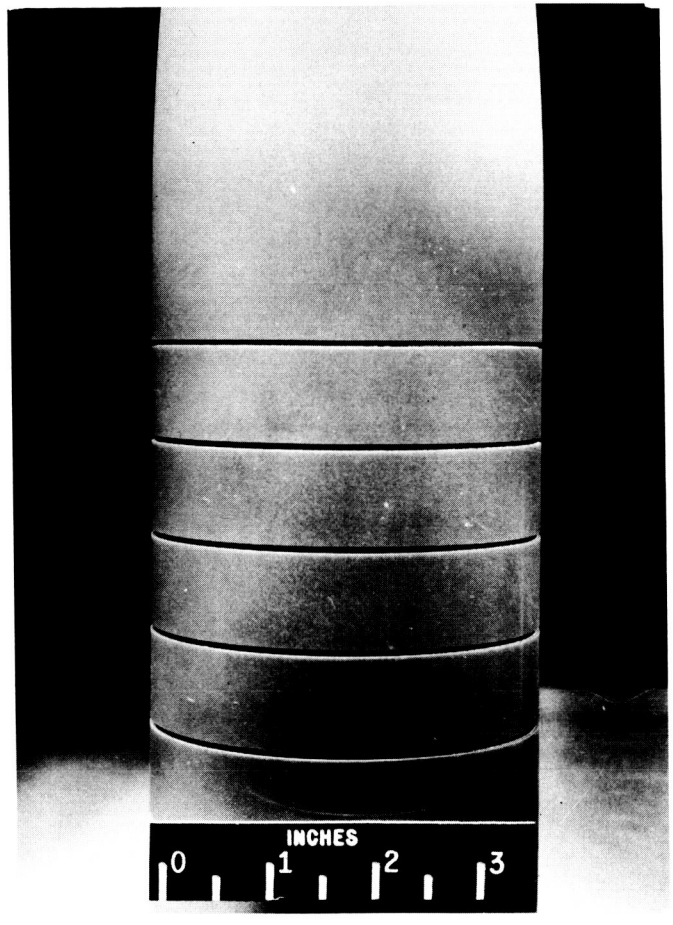

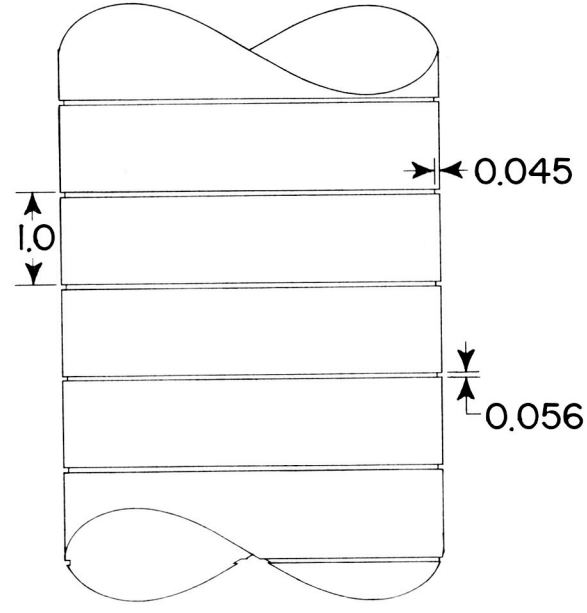

(h) 0.056-inch transverse grooves. L-63-3120

Figure 3.- Continued.

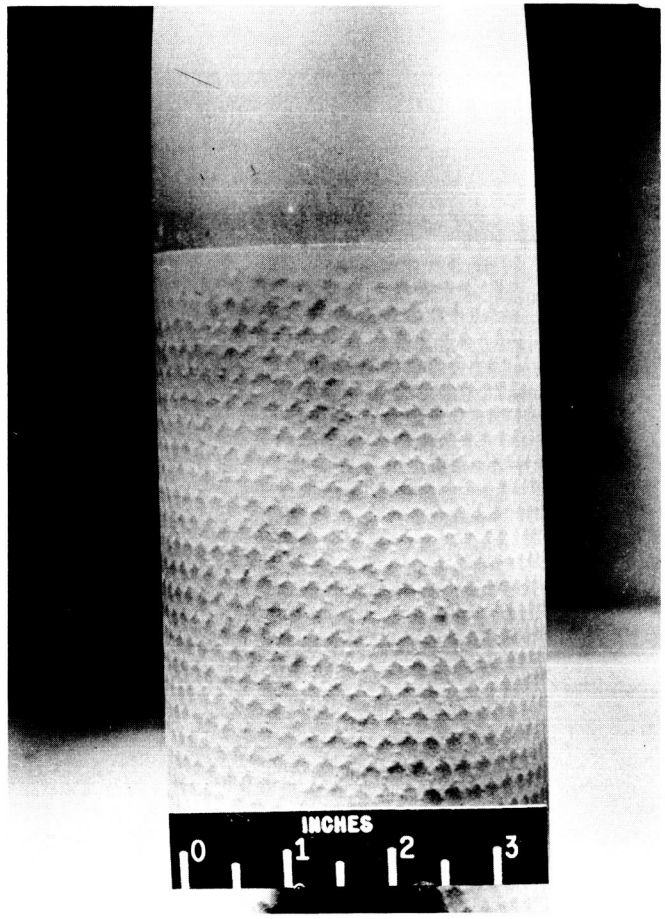

(i) Coarse irregular waffle.

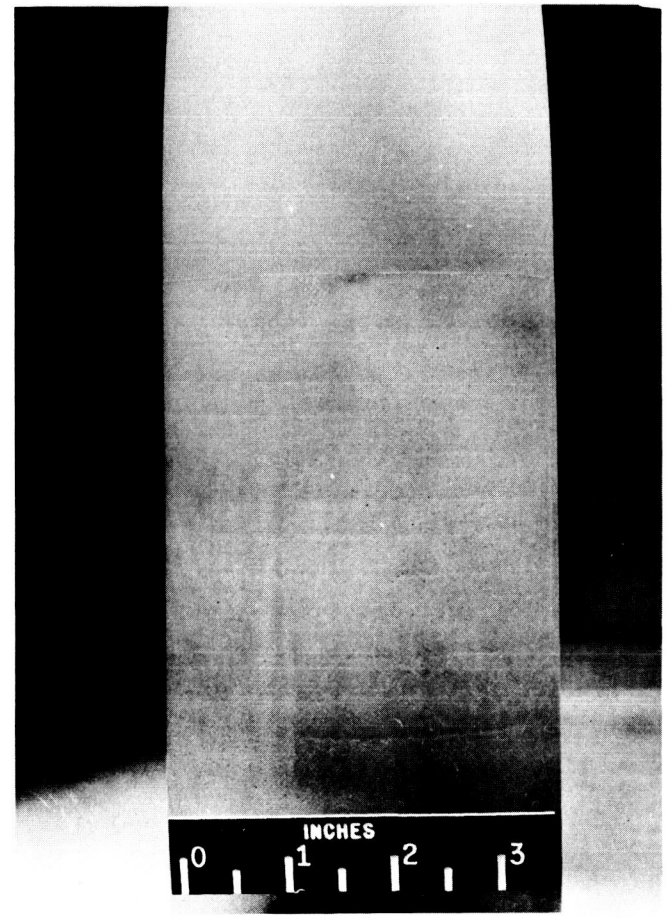

L-63-3121

(j) Coarse circumferential hemstitching.

Figure 3.- Concluded.

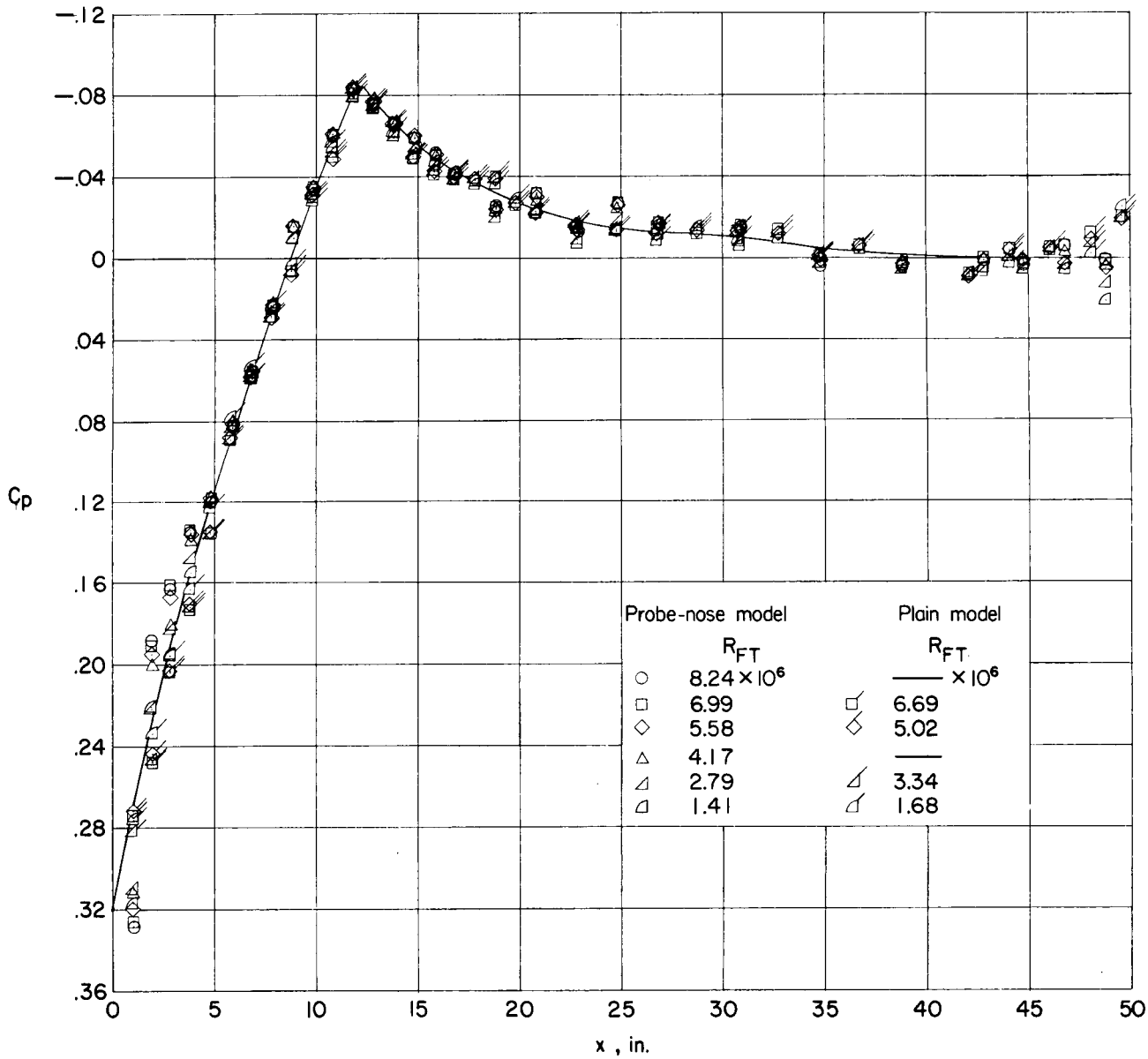

Figure 4.- Pressure distributions over basic smooth models. M = 1.61.

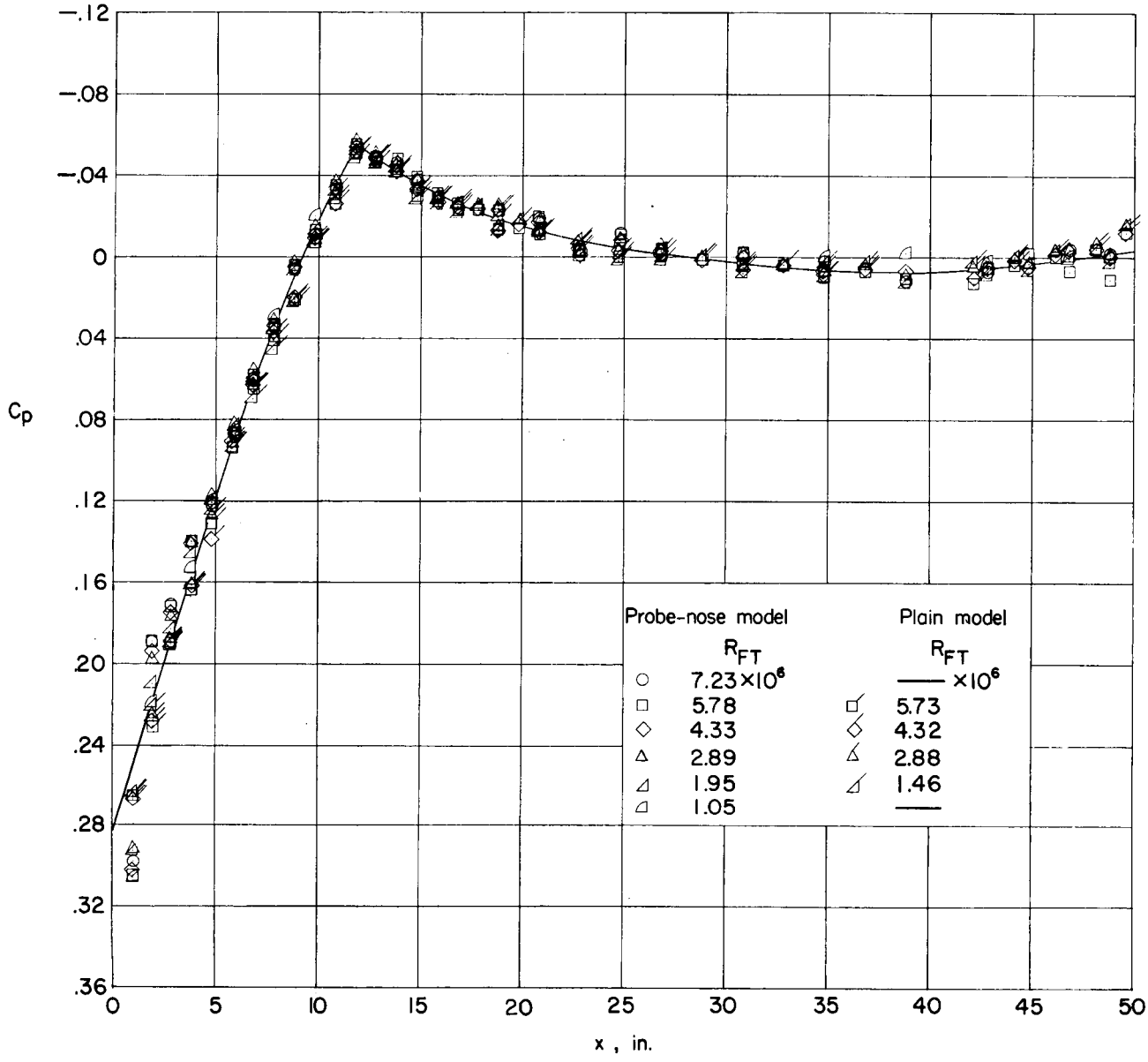

Figure 5.- Pressure distributions over basic smooth models. M = 2.01.

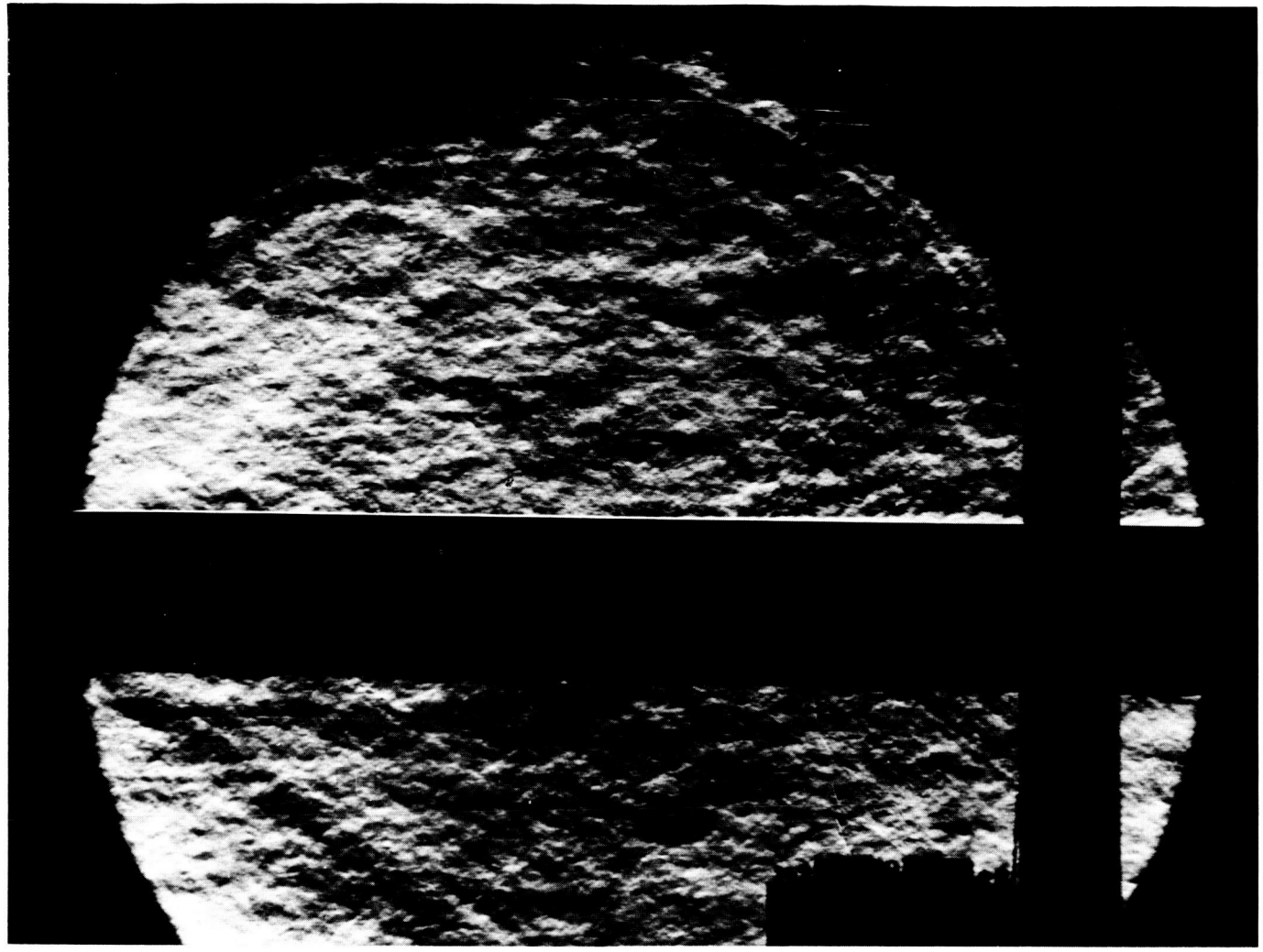

(a) Smooth waffle. $R_{FT} = 3.29 \times 10^6$. L-63-3122

Figure 6.- Typical schlieren photographs showing boundary-layer transition. M = 1.61.

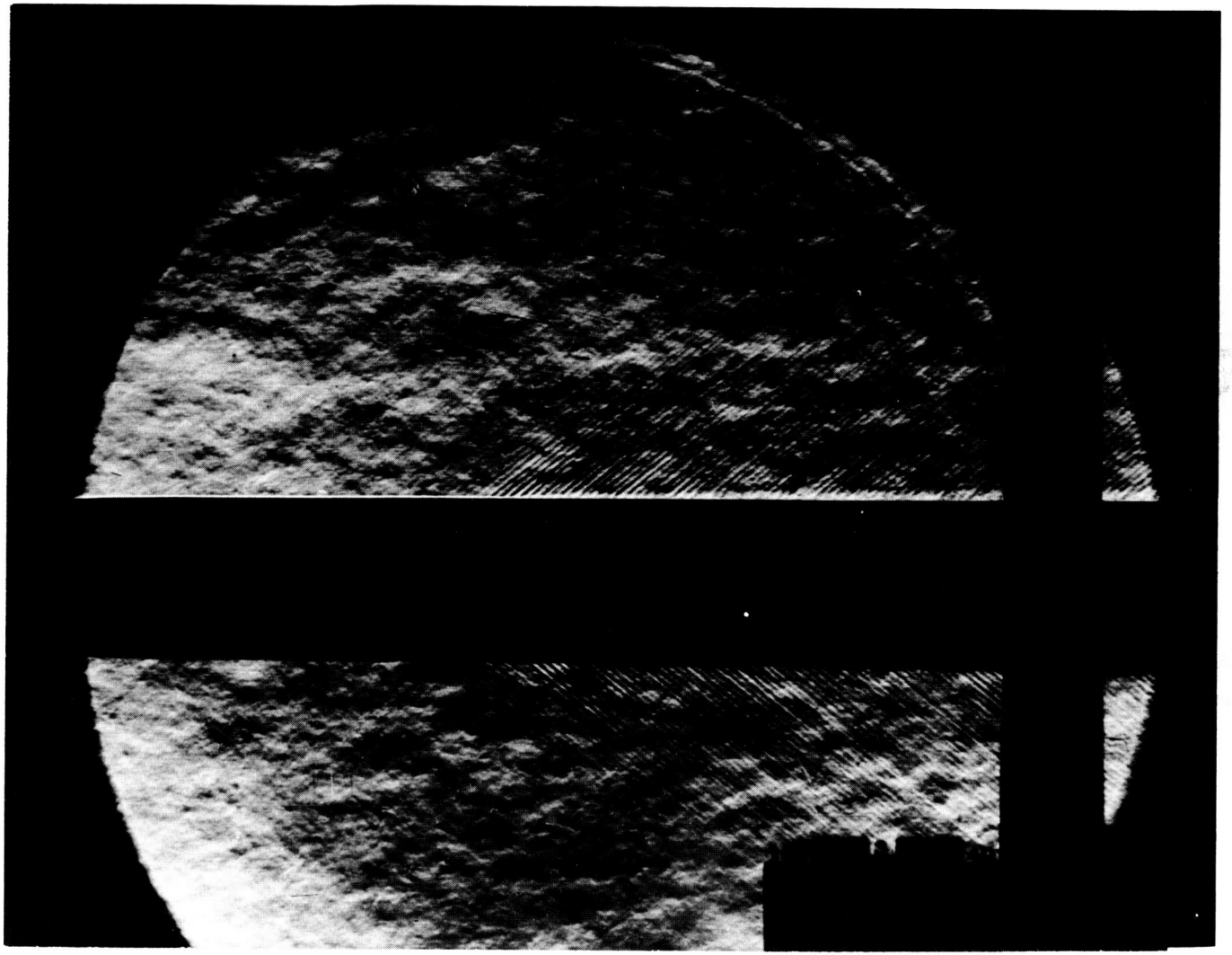

(b) Coarse irregular waffle. $R_{FT} = 2.07 \times 10^6$. L-63-3123

Figure 6.- Continued.

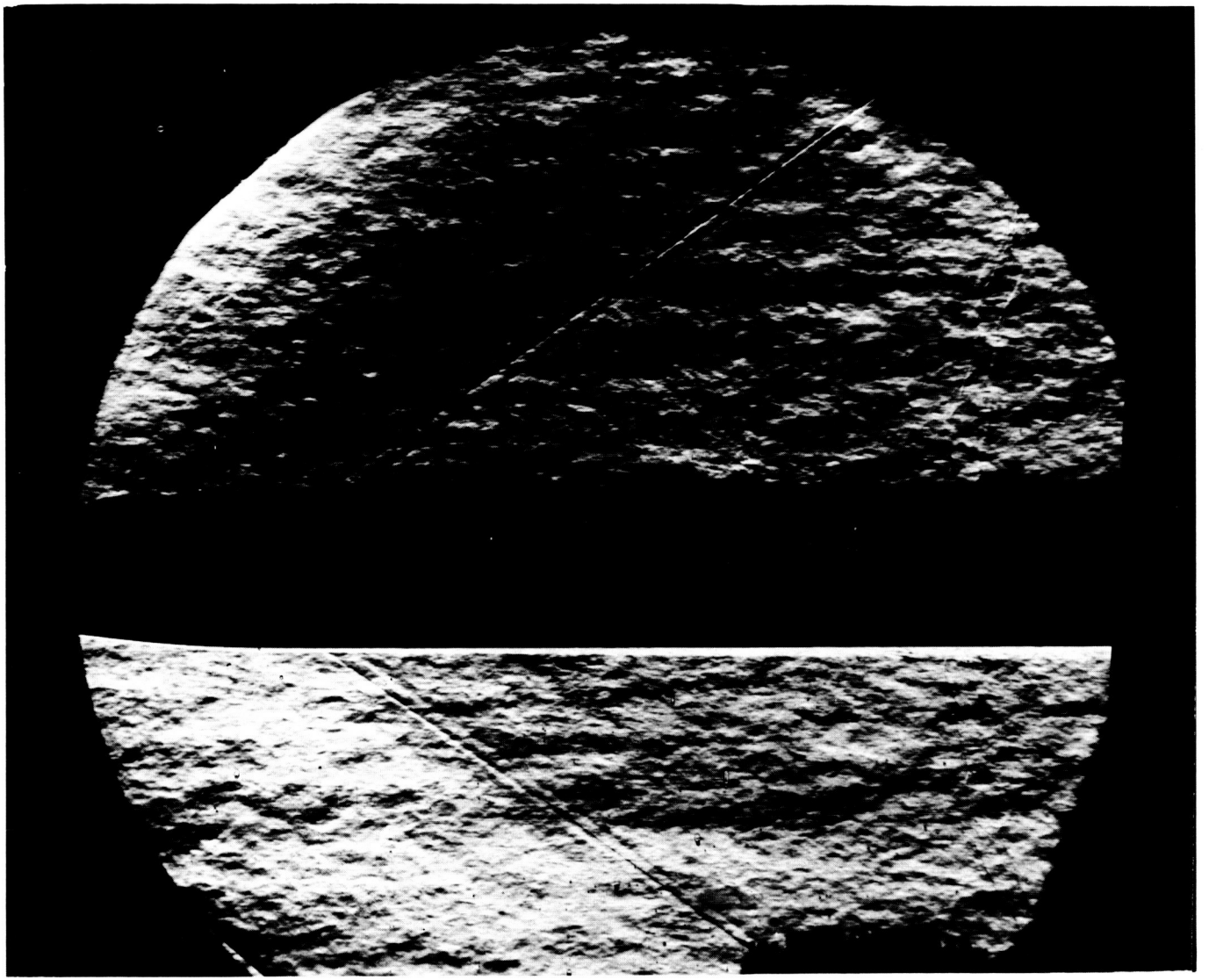

(c) 0.059-inch longitudinal grooves. $R_{FT} = 3.40 \times 10^6$. L-63-3124

Figure 6.- Continued.

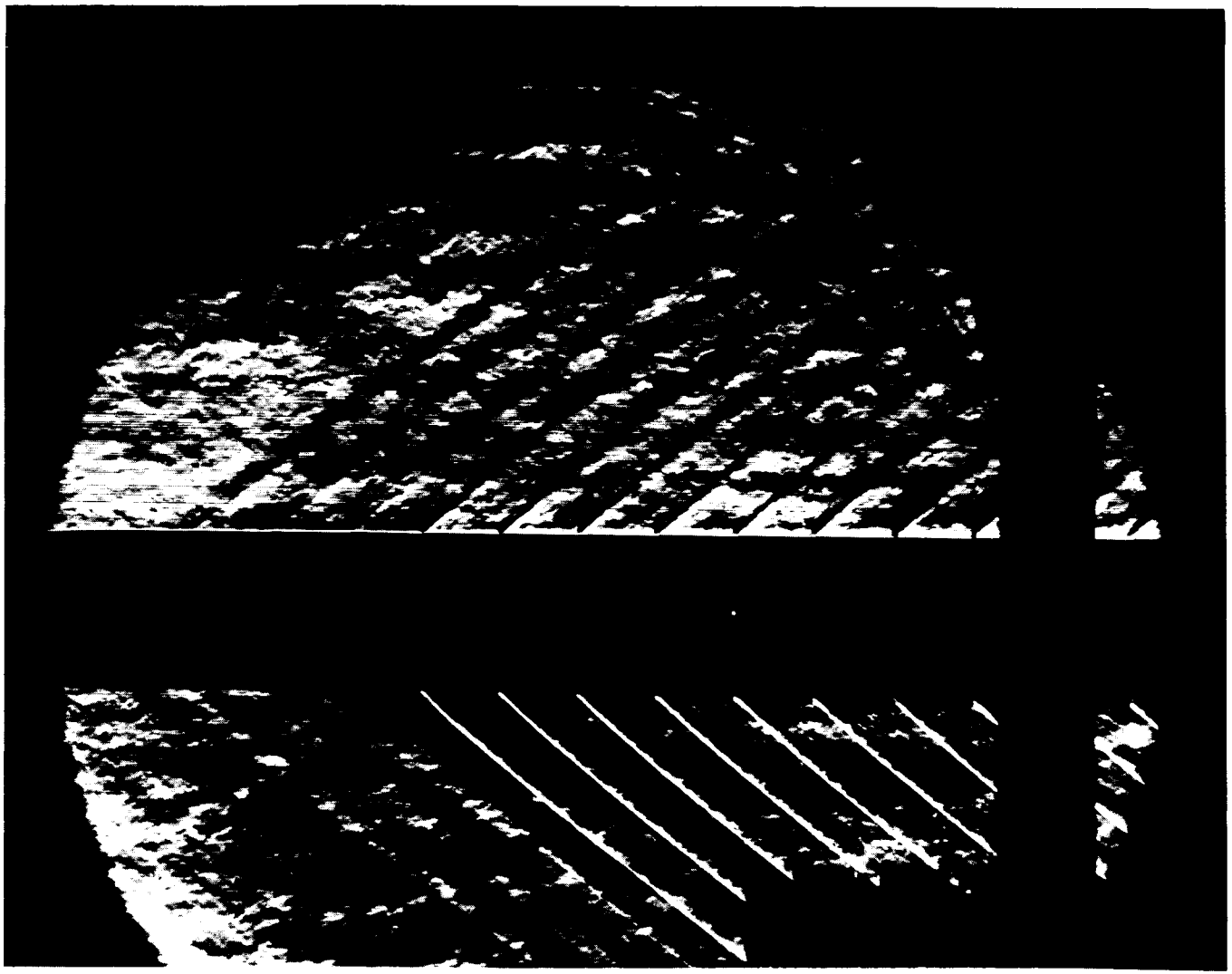

(d) 0.020-inch forward steps. $R_{FT} = 3.92 \times 10^6$. L-63-3125

Figure 6.- Continued.

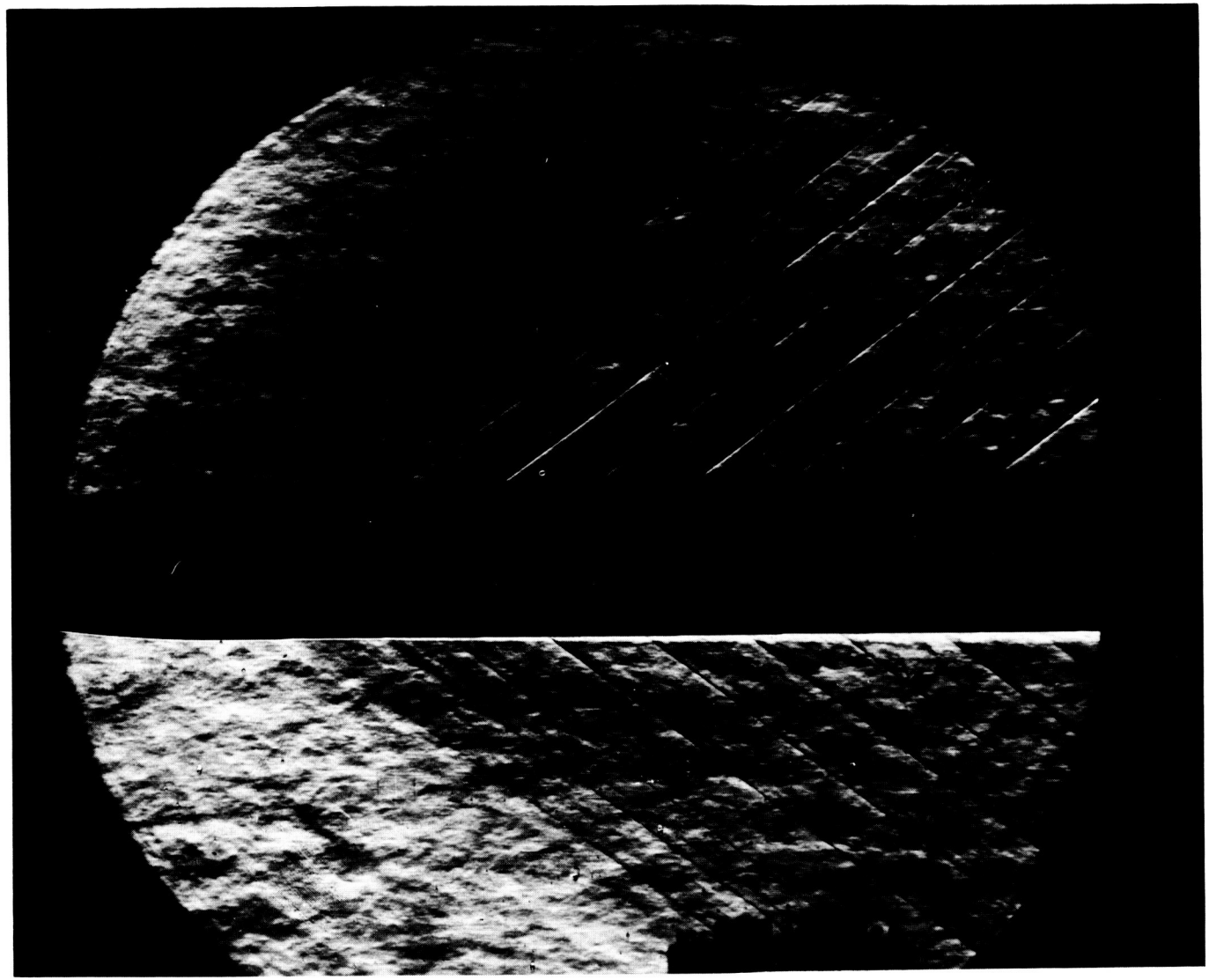

(e) 0.020-inch 45° rearward steps. $R_{FT} = 4.04 \times 10^6$. L-63-3126

Figure 6.- Continued.

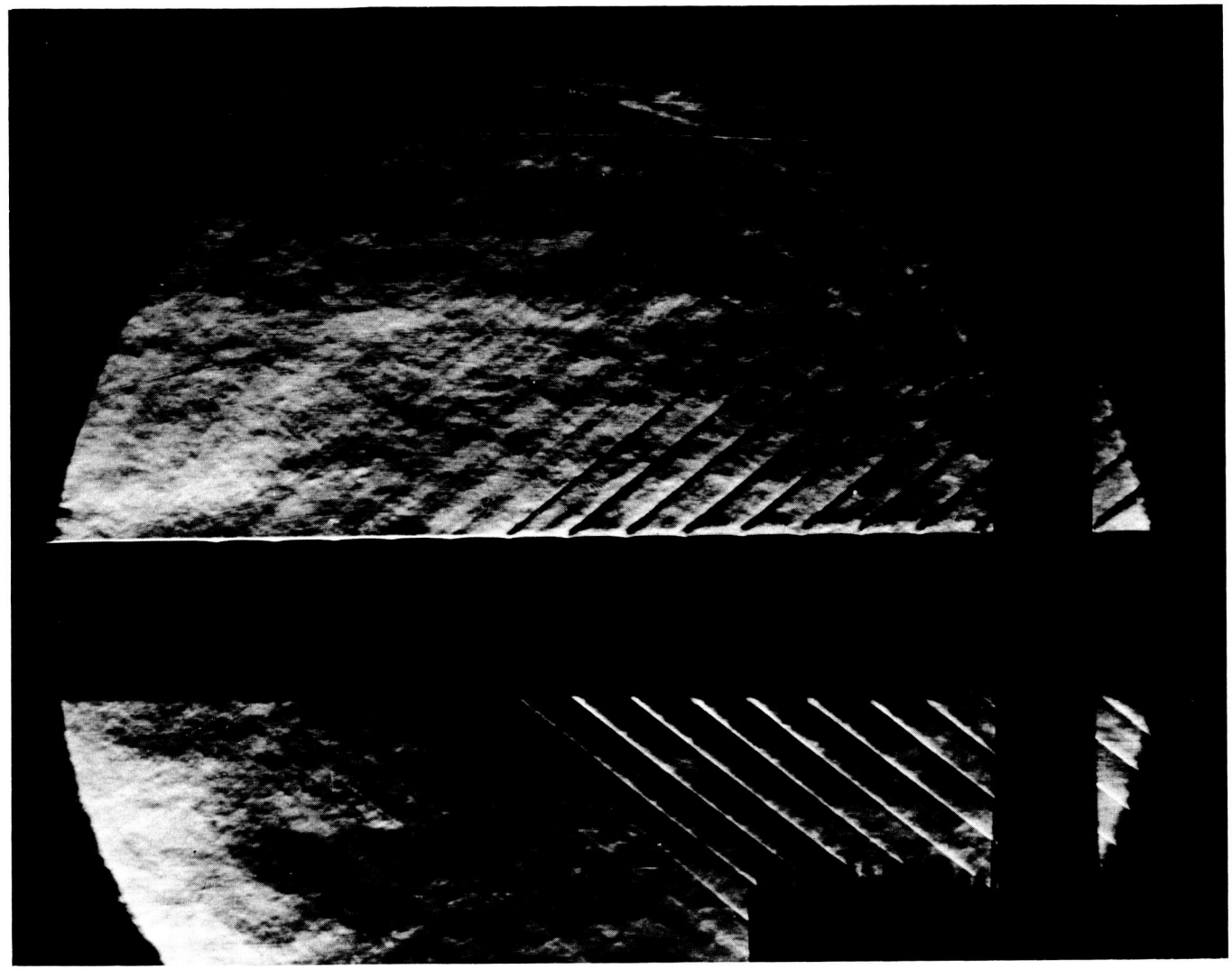

(f) 0.053-inch transverse creases. $R_{FT} = 1.48 \times 10^6$. L-63-3127

Figure 6.- Concluded.

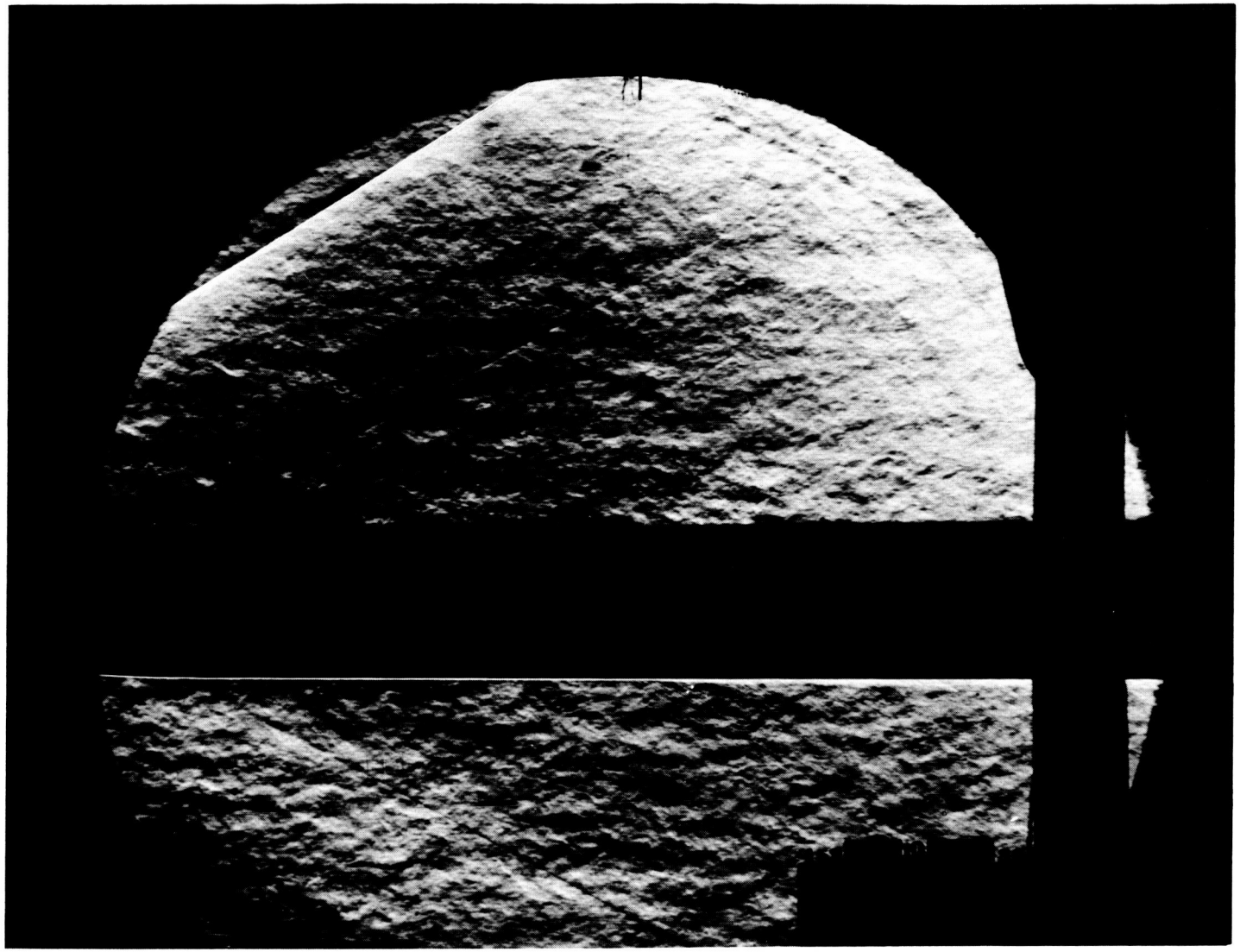

(a) Coarse longitudinal hemstitching. $R_{FT} = 3.94 \times 10^6$. L-63-3128

Figure 7.- Typical schlieren photographs showing boundary-layer transition. M = 2.01.

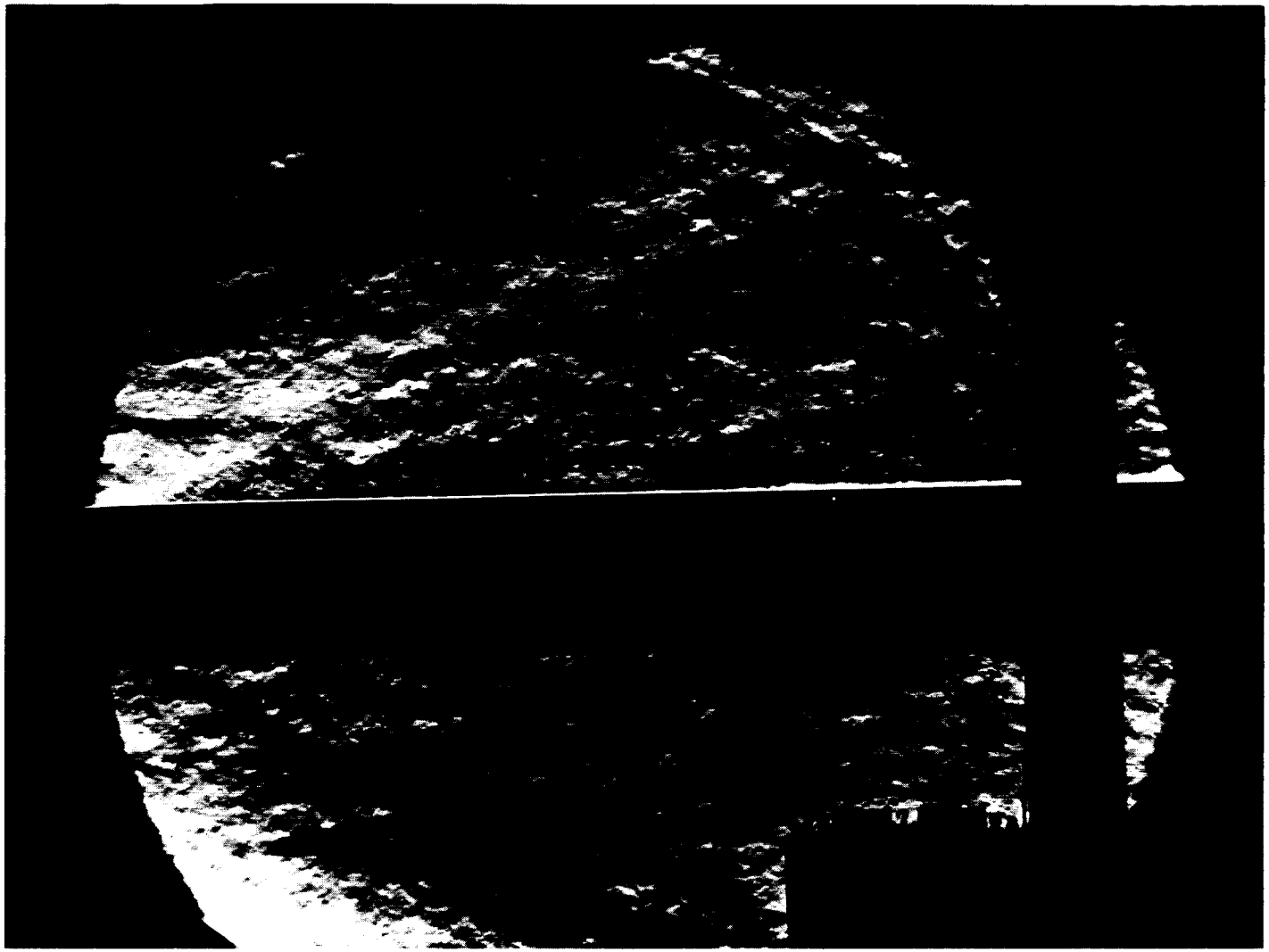

(b) Smooth waffle. $R_{FT} = 3.69 \times 10^6$. L-63-3129

Figure 7.- Continued.

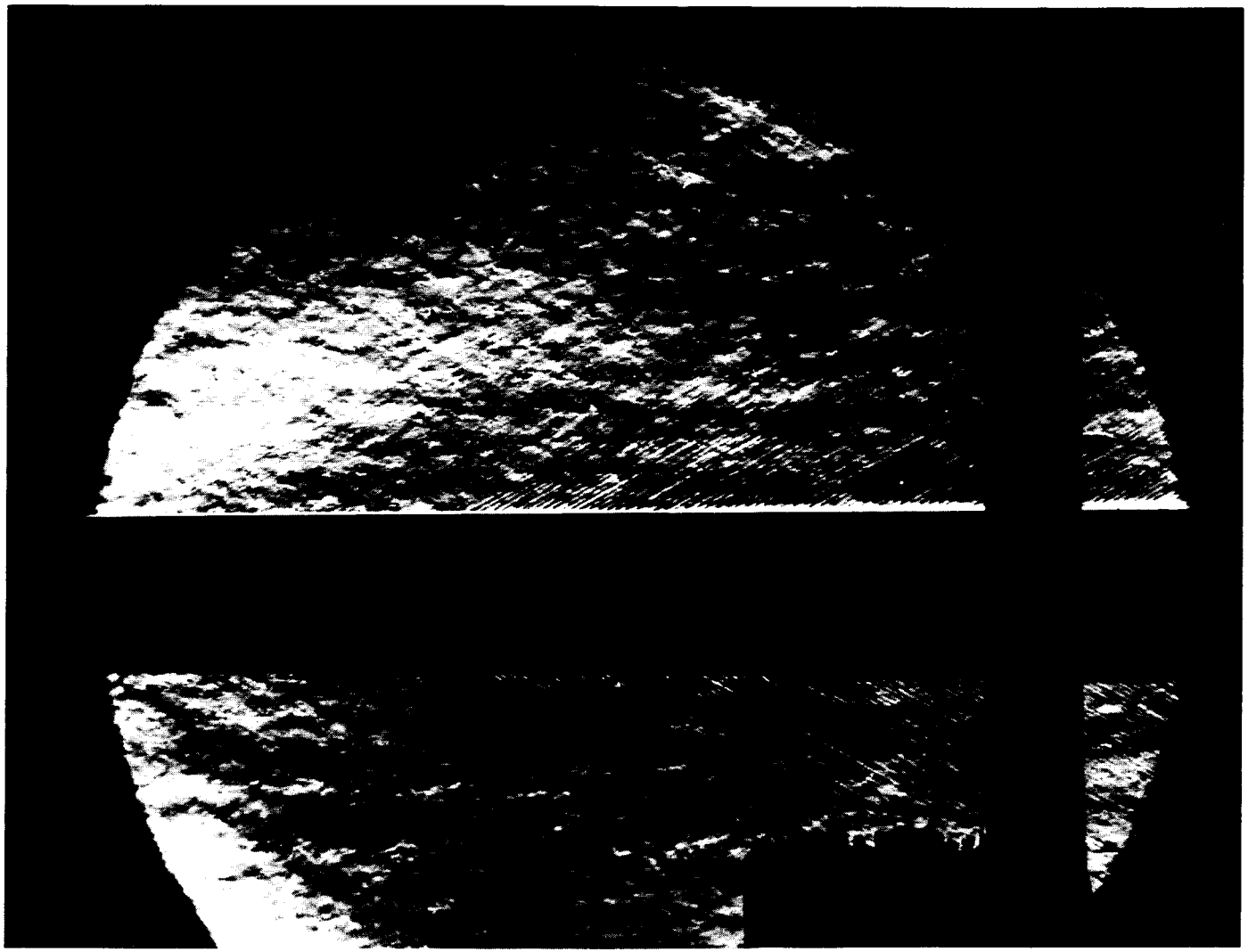

(c) Coarse irregular waffle. $R_{FT} = 2.86 \times 10^6$. L-63-3130

Figure 7.- Continued.

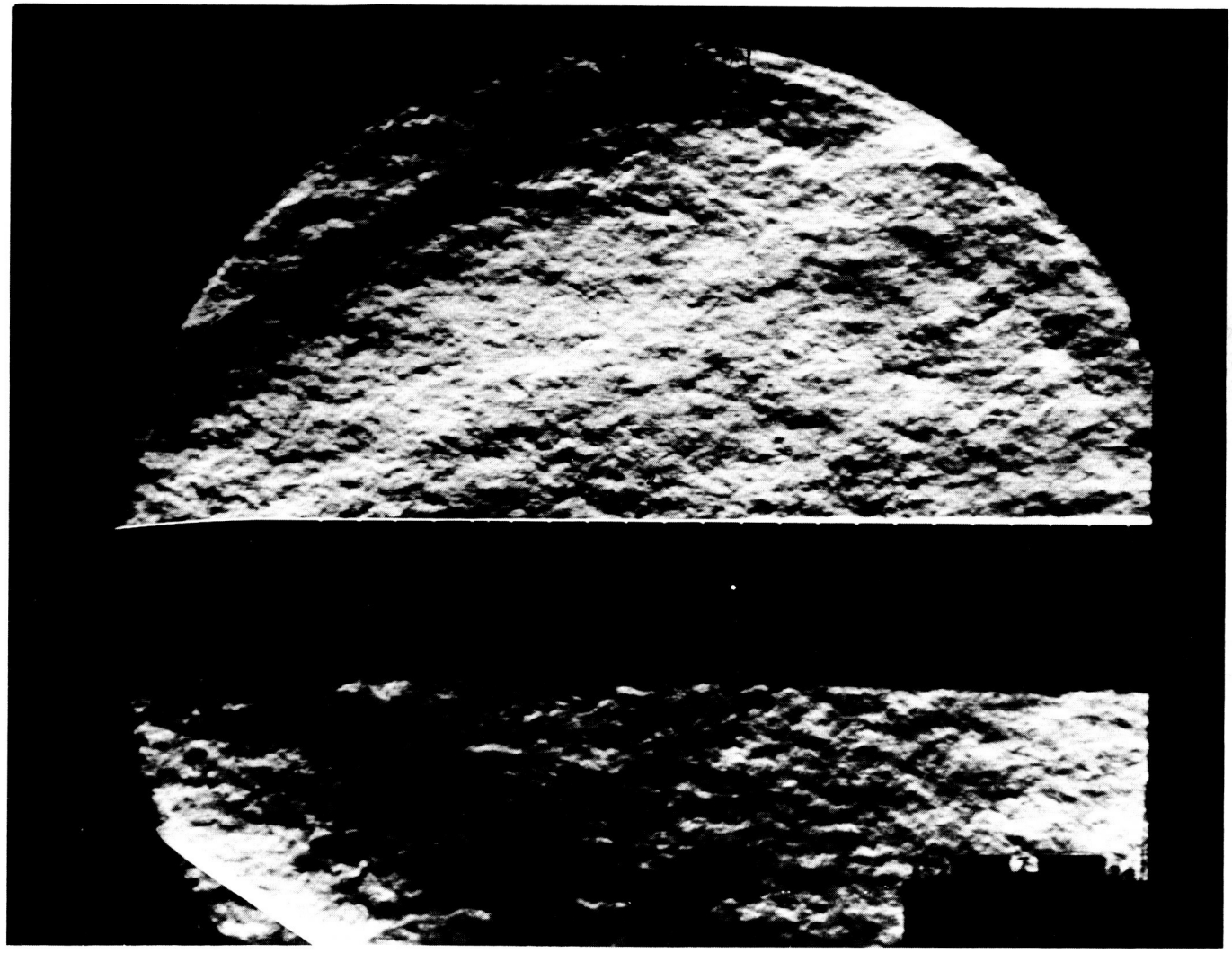

(d) 0.056-inch transverse grooves. $R_{FT} = 3.66 \times 10^6$. L-63-3131

Figure 7.- Continued.

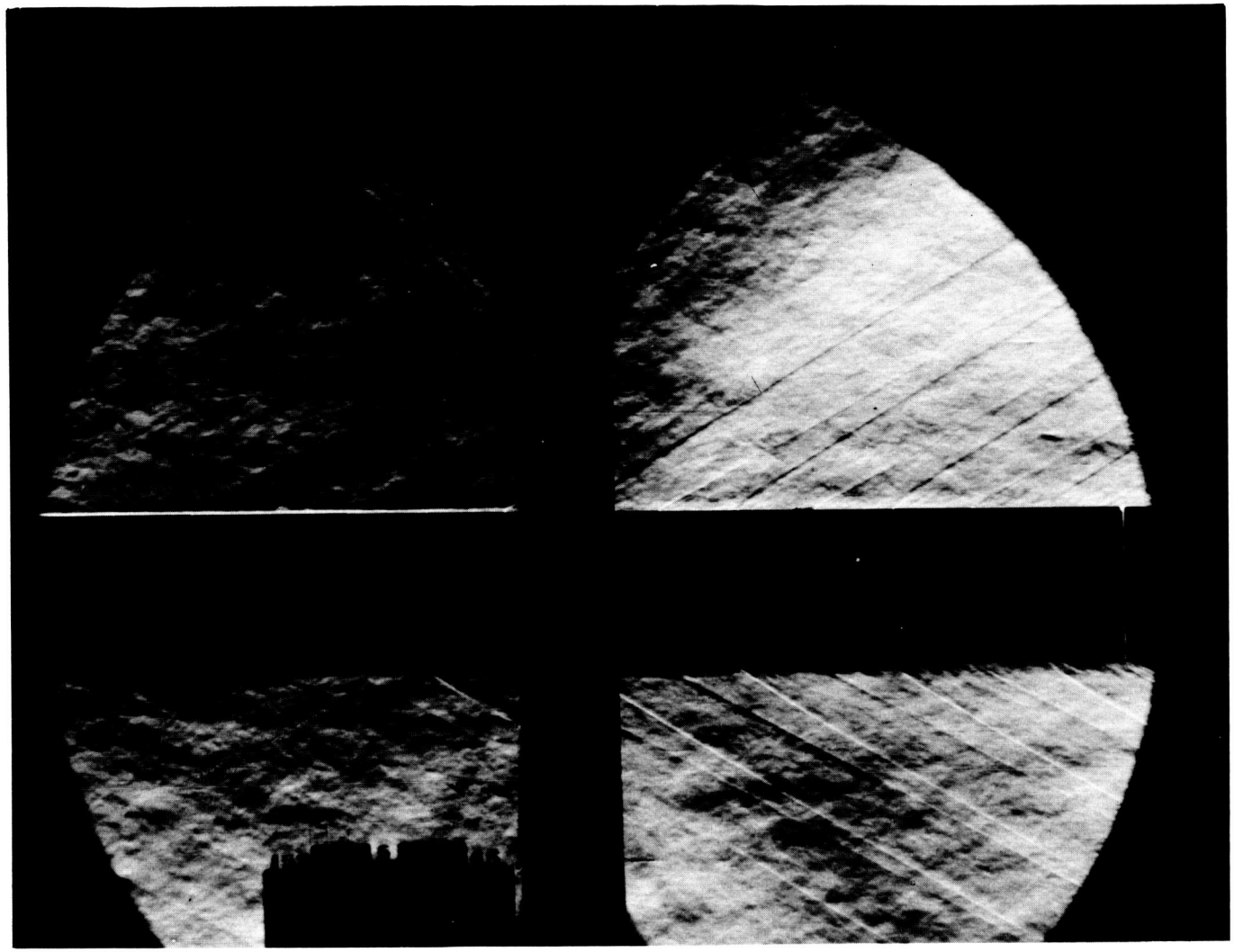

(e) 0.010-inch steps with grooves. $R_{FT} = 1.71 \times 10^6$. L-63-3132

Figure 7.- Continued.

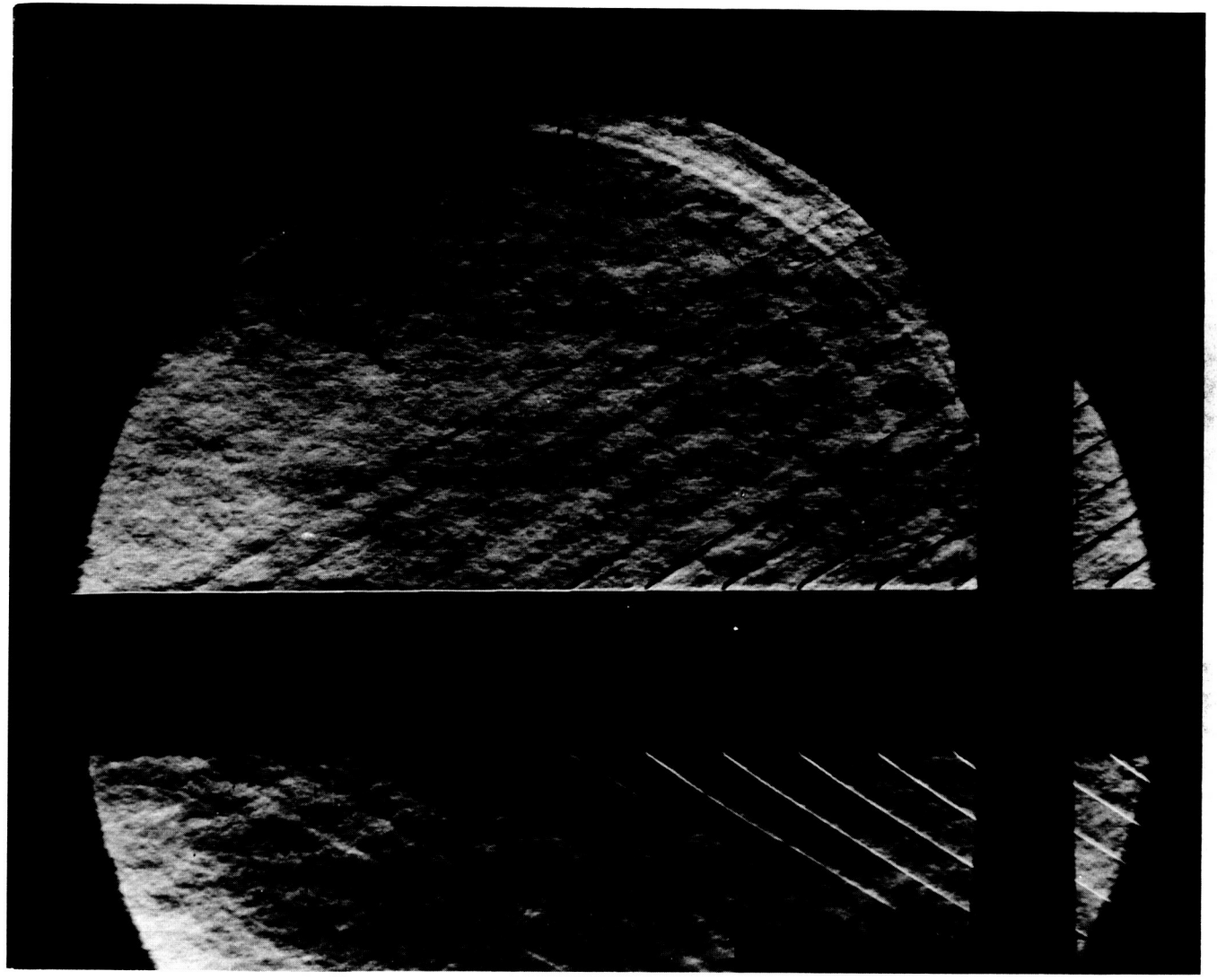

(f) 0.020-inch forward steps. $R_{FT} = 2.16 \times 10^6$. L-63-3133

Figure 7.- Continued.

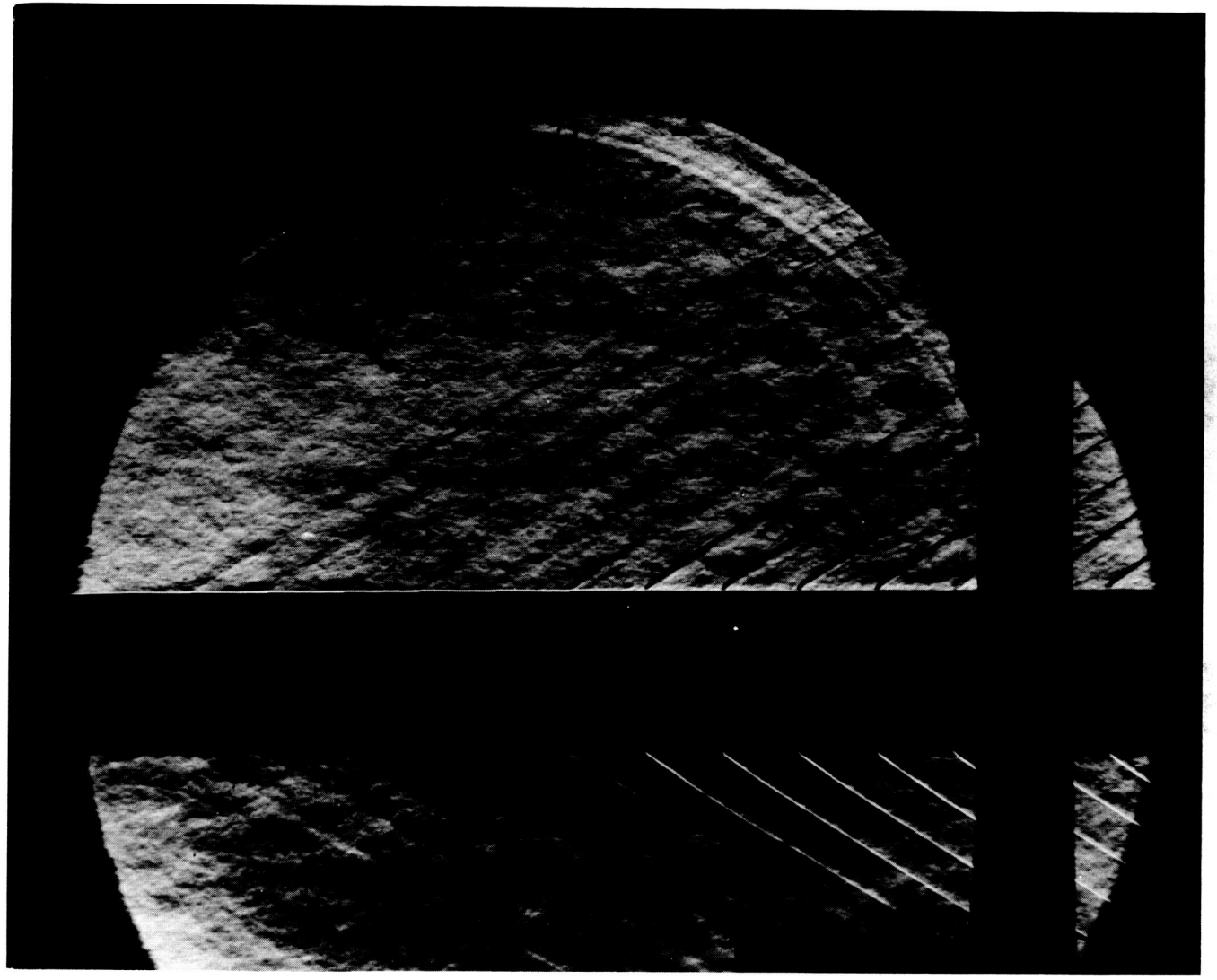

(f) 0.020-inch forward steps. $R_{FT} = 2.16 \times 10^6$. L-63-3133

Figure 7.- Continued.

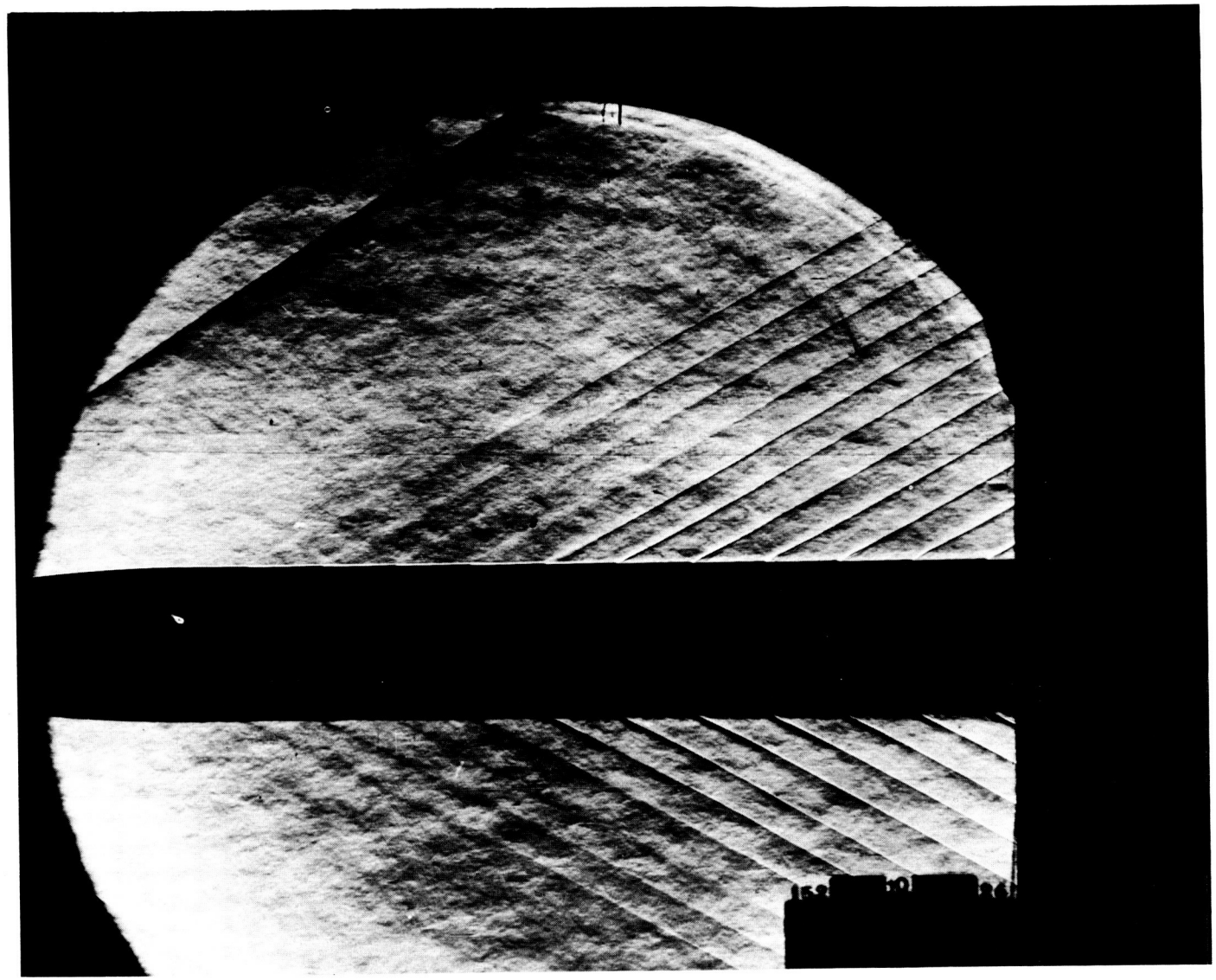

(g) 0.021-inch rearward steps. $R_{FT} = 2.86 \times 10^6$. L-63-3134

Figure 7.- Continued.

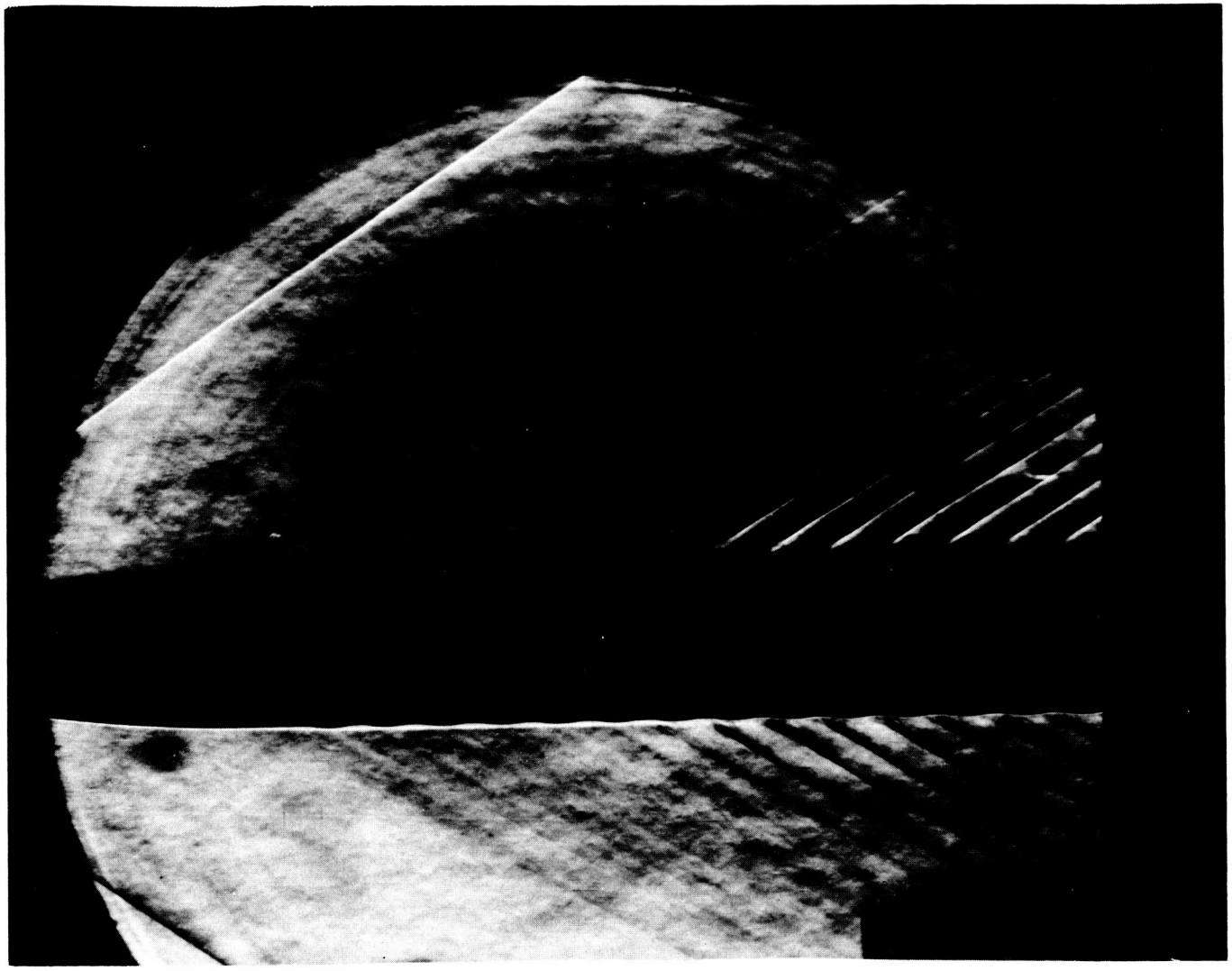

(h) 0.053-inch protruding waves. $R_{FT} = 0.90 \times 10^6$. L-63-3135

Figure 7.- Continued.

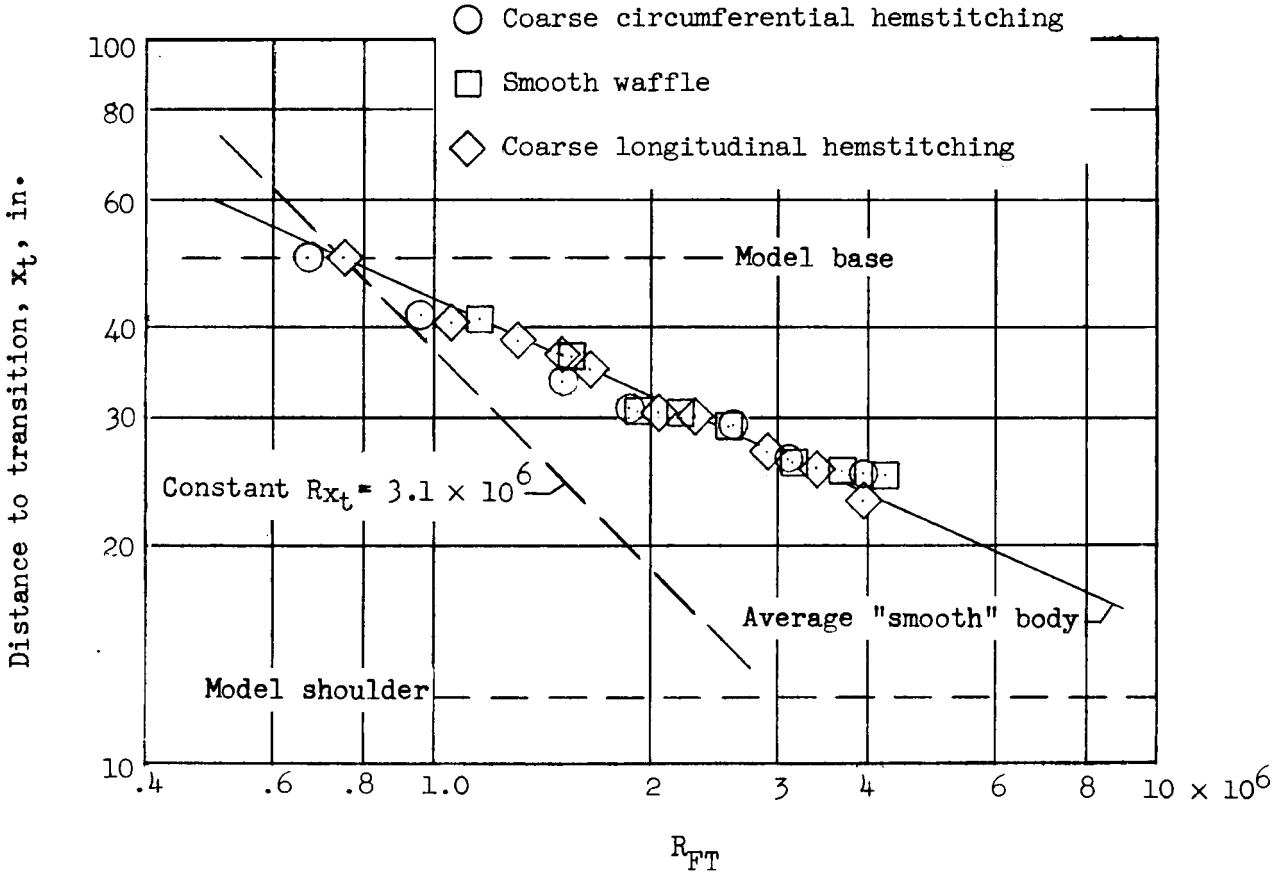

Figure 8.- Determination of reference transition curve for "smooth" body. M = 2.01.

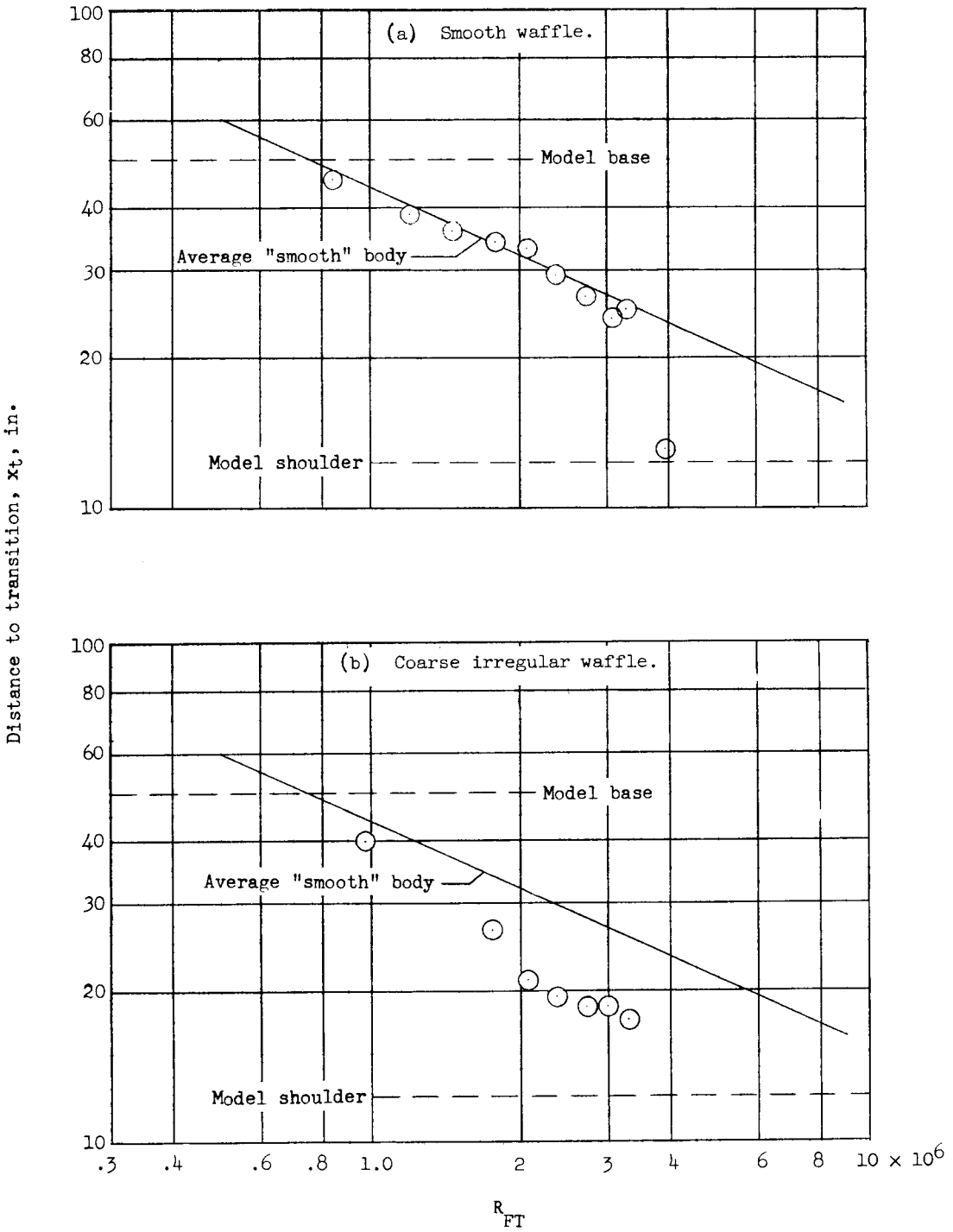

Figure 9.- Variation of distance to transition x_t with free-stream Reynolds number per foot R_{FT} for various types of surface roughness. M = 1.61.

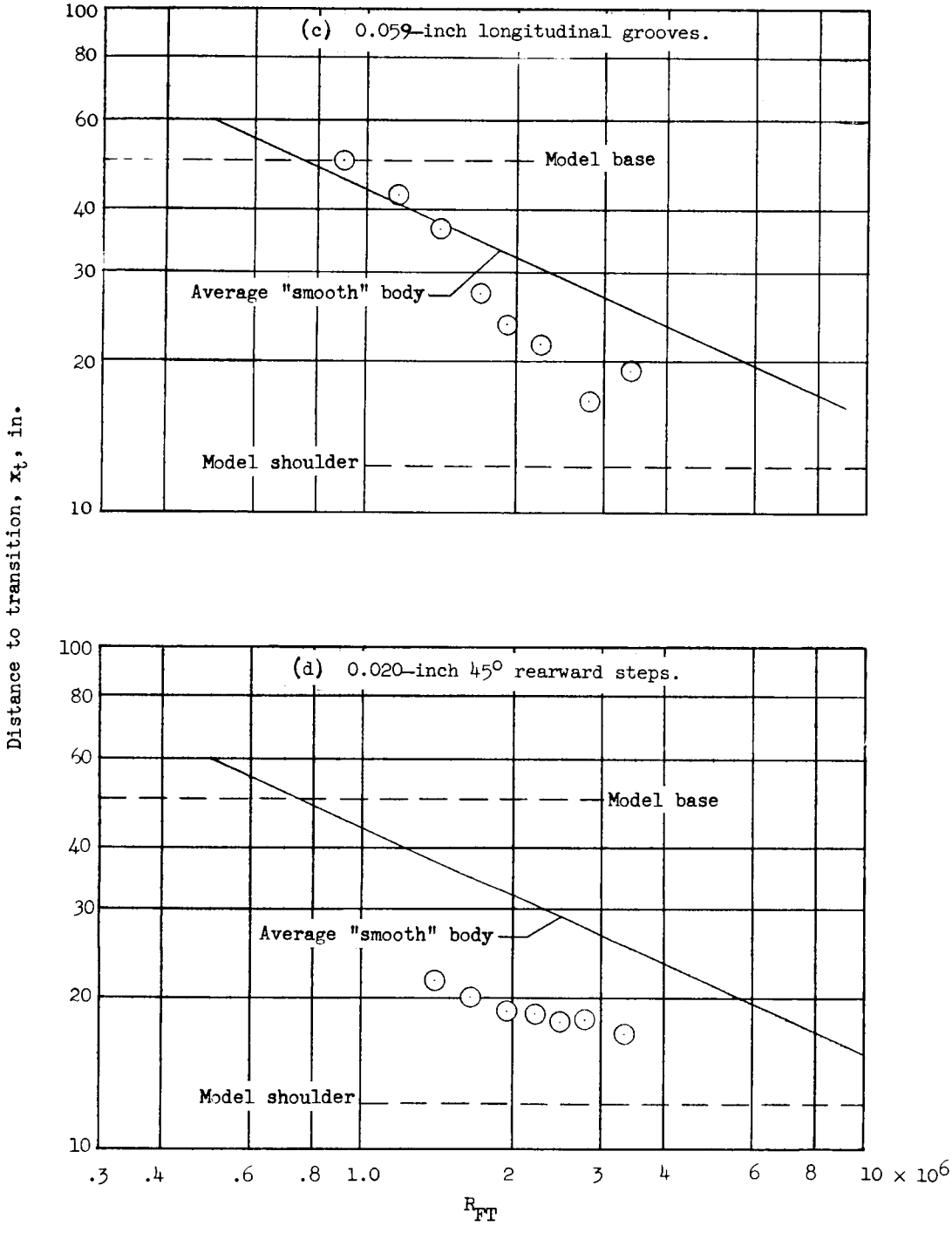

Figure 9.- Continued.

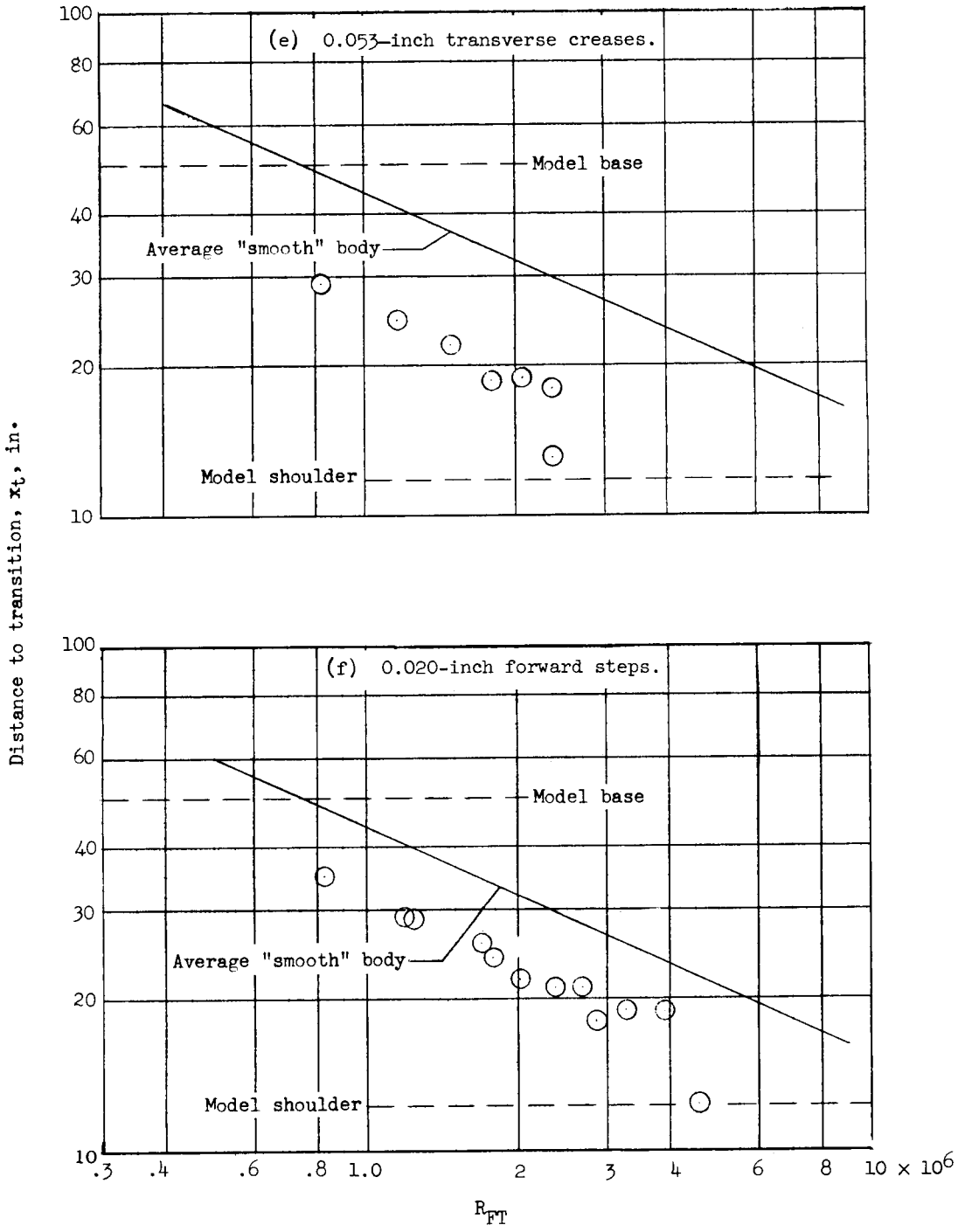

Figure 9.- Concluded.

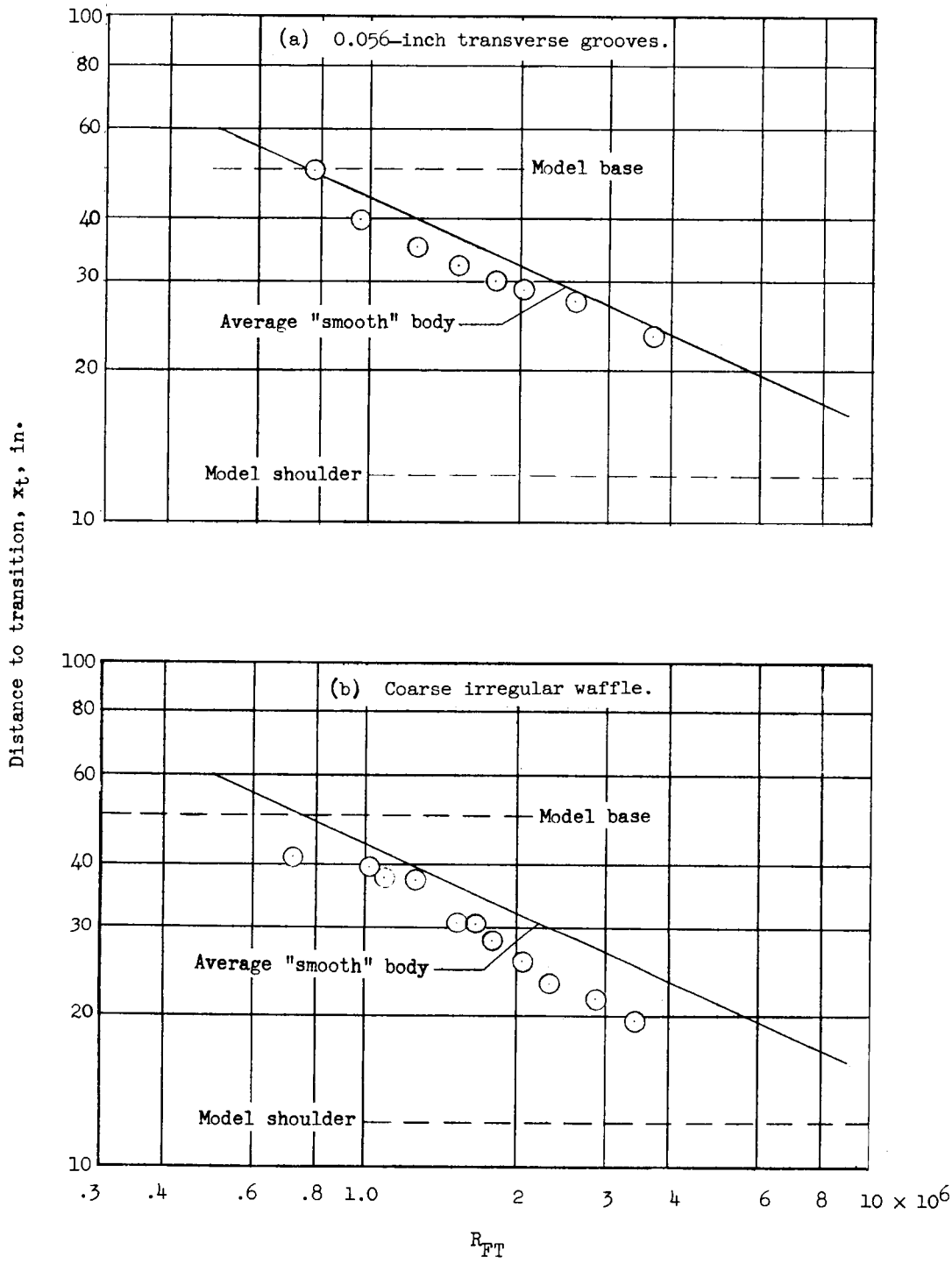

Figure 10.- Variation of distance to transition x_t with free-stream Reynolds number per foot R_{FT} for various types of surface roughness. M = 2.01.

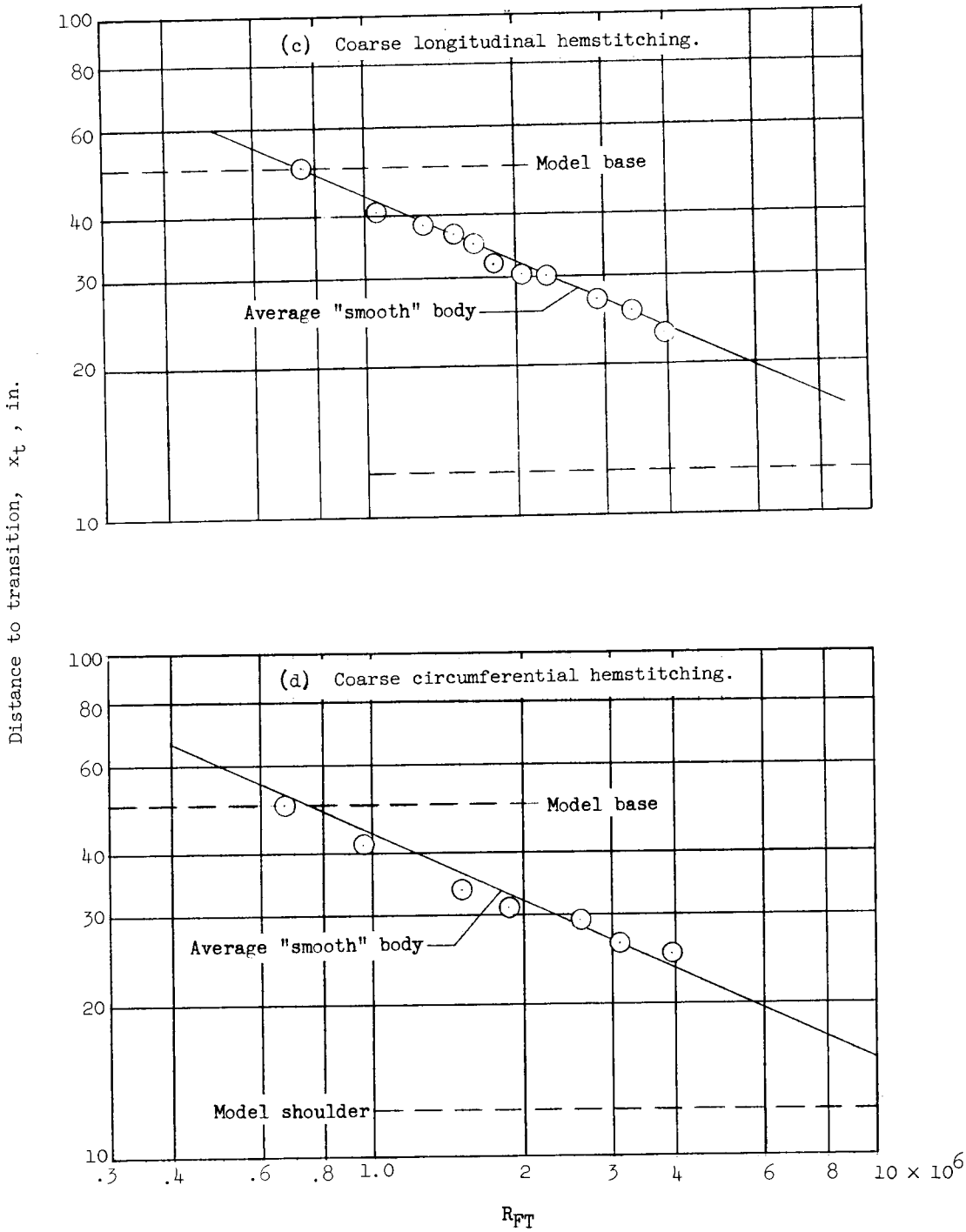

Figure 10.- Continued.

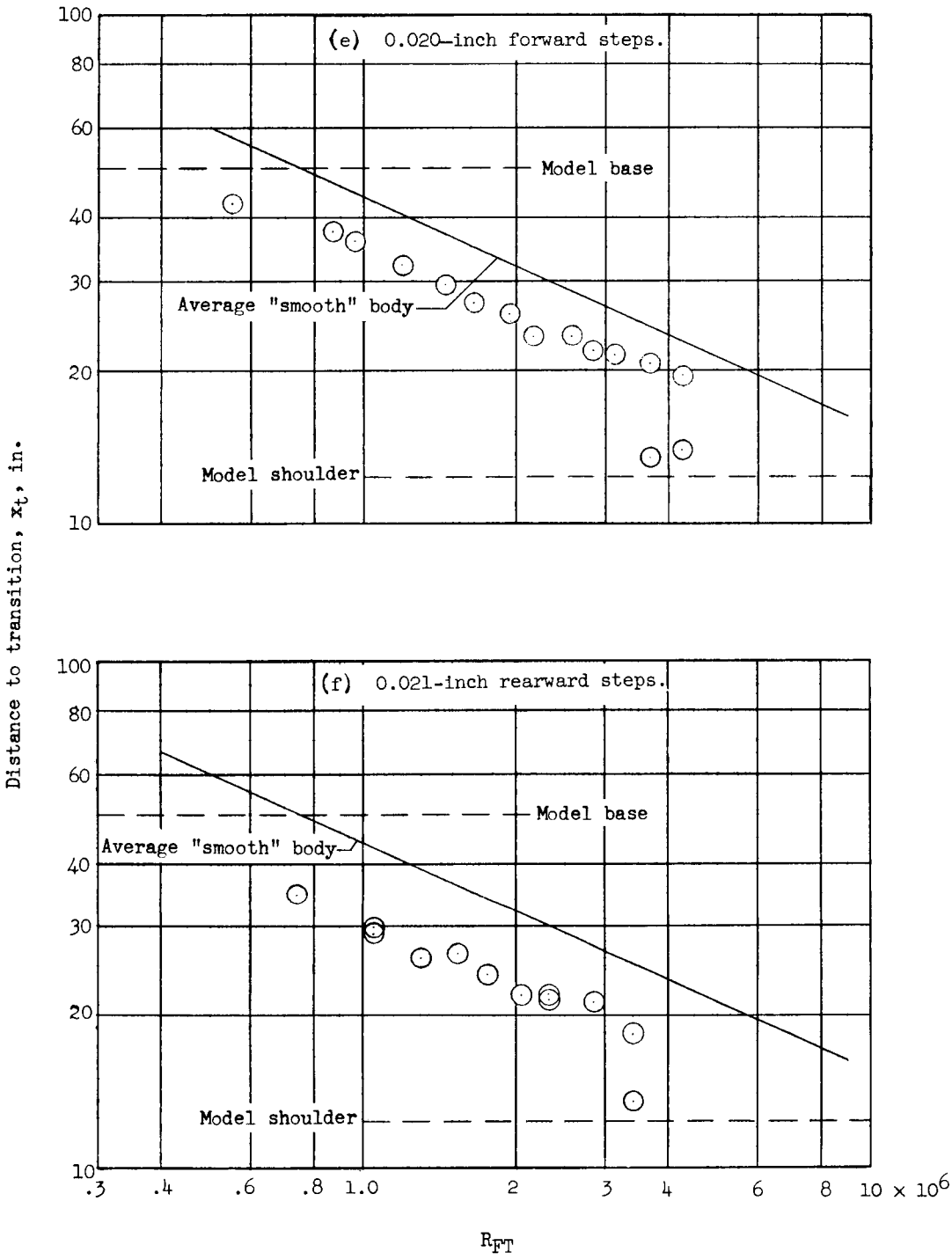

Figure 10.- Continued.

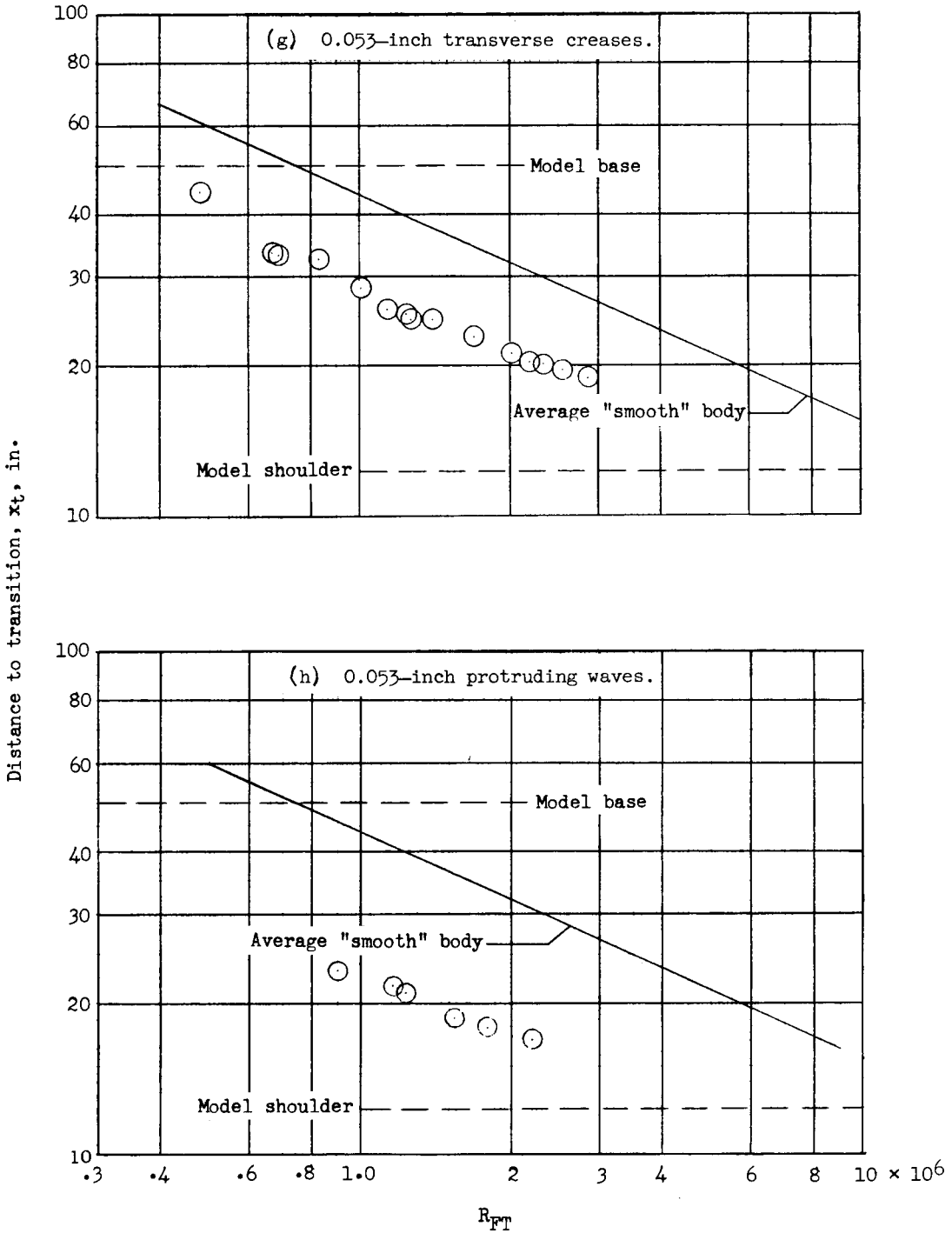

Figure 10.- Continued.

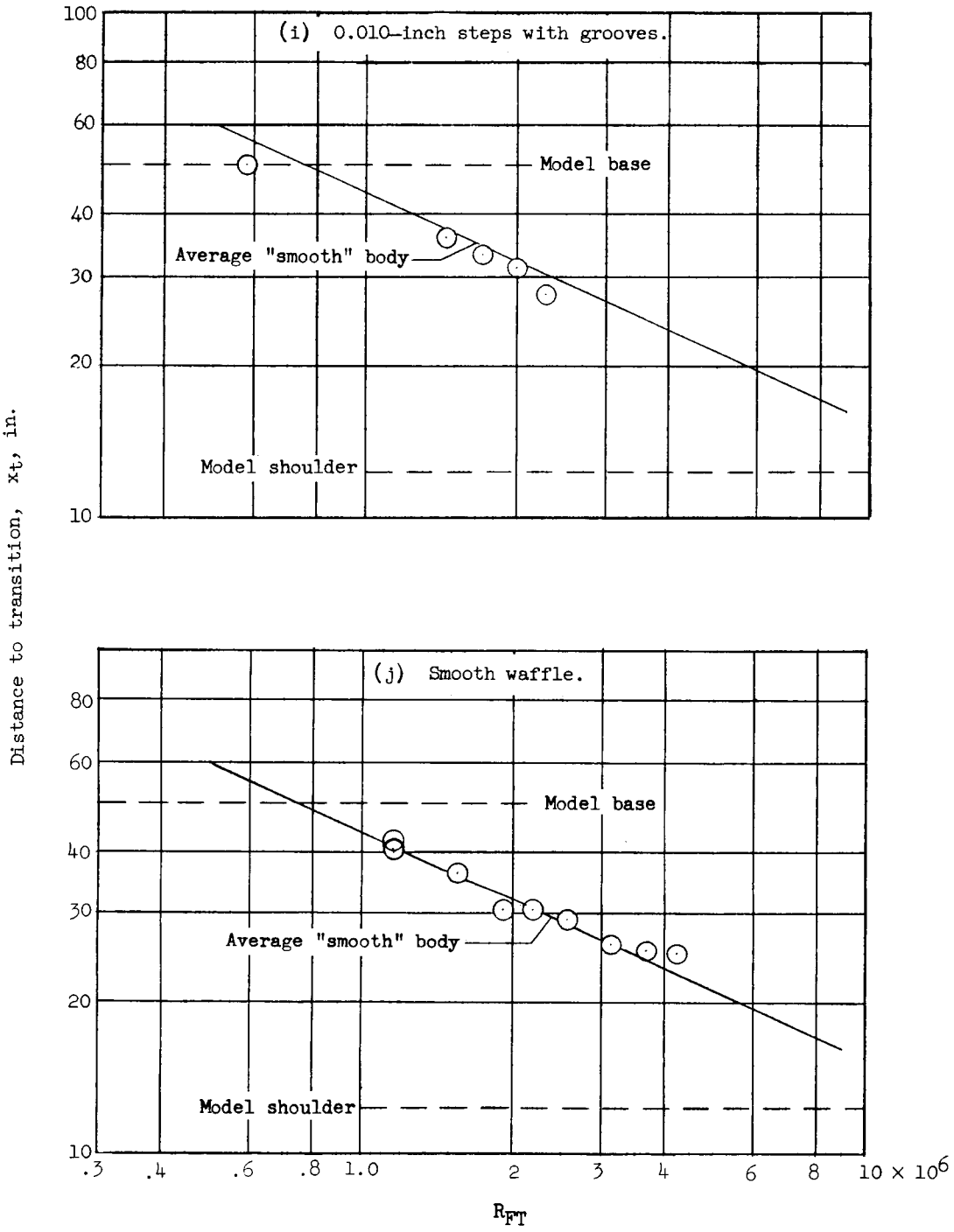

Figure 10.- Concluded.

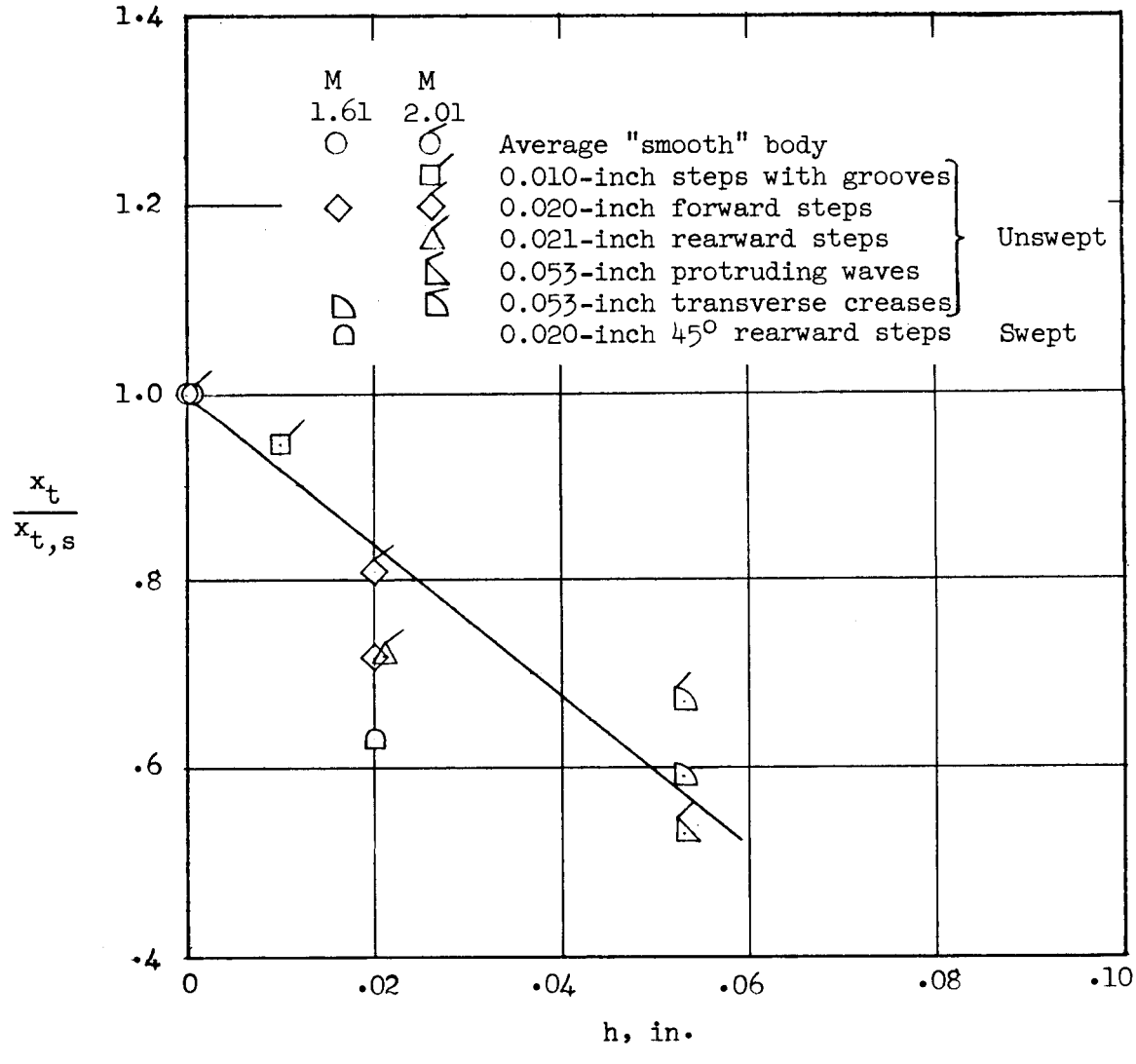

Figure 11.- Variation of transition-distance ratio $x_t/x_{t,s}$ with height of two-dimensional protruding swept and unswept surface roughness h.